



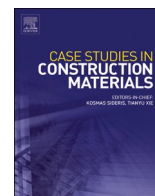
## **Characterization, activation and reactivity – A case study of Nordic volcanic materials for application as Supplementary Cementitious**

Downloaded from: <https://research.chalmers.se>, 2025-01-20 04:34 UTC

Citation for the original published paper (version of record):

Hazarika, A., Huang, L., Erlingsson, S. et al (2025). Characterization, activation and reactivity – A case study of Nordic volcanic materials for application as Supplementary Cementitious Materials. *Case Studies in Construction Materials*, 22. <http://dx.doi.org/10.1016/j.cscm.2024.e04096>

N.B. When citing this work, cite the original published paper.



## Characterization, activation and reactivity – A case study of Nordic volcanic materials for application as Supplementary Cementitious Materials

Amrita Hazarika<sup>a,\*</sup>, Liming Huang<sup>a</sup>, Sigurdur Erlingsson<sup>b,c</sup>, Klaartje de Weerd<sup>d</sup>, Ingemar Löfgren<sup>a,e</sup>, Sahar Iftikhar<sup>a</sup>, Arezou Babaahmadi<sup>a</sup>

<sup>a</sup> Department of Architecture and Civil Engineering, Chalmers University of Technology, Gothenburg, Sweden

<sup>b</sup> Faculty of Civil and Environmental Engineering, University of Iceland, Reykjavik, Iceland

<sup>c</sup> VTI, The Swedish National Road and Transport Research Institute, Linköping, Sweden

<sup>d</sup> Department of Structural Engineering, Norwegian University of Science and Technology, Trondheim, Norway

<sup>e</sup> Thomas Concrete Group AB, Gothenburg, Sweden

### ARTICLE INFO

#### Keywords:

Volcanic material  
Mechanochemical Activation  
Size distribution  
Specific surface areas  
Mineralogy  
Reactivity

### ABSTRACT

Despite their historical importance, the widespread use of volcanic materials as Supplementary Cementitious Materials faces challenges. There exists a knowledge gap relating the properties such as chemical compositions, mineralogy, physical attributes (effective particle size distribution, and specific surface areas) with reactivity. The current study investigates the correlation between noted properties when physical properties are altered by mechanochemical treatments applied to four unique volcanic materials with diverse mineralogy including Albite, Anorthite, Andesine, Oligoclase and Olivine. The alterations in these properties are then linked to changes in the reactivity levels of volcanic materials. The key findings emphasize that grinding volcanic materials for up to 20 min can result in significant improvements. The following outlines the most notable changes observed from 5 min to 20 min: a decrease in D50 from 37  $\mu\text{m}$  to 9  $\mu\text{m}$ , an increase in surface area from 4  $\text{m}^2/\text{g}$  to 13  $\text{m}^2/\text{g}$ , and a rise in average degree of amorphization of the four volcanic materials from 70 % to 83 %. Progressive increases in reactivity levels were observed when extending the milling time from 5 to 20 min, with the most significant increase showing a change from 56 J/g to 350 J/g SCM, as measured with the MR3 reactivity test. X-ray diffraction analyses reveal the detection of new phases like Magnetite and Iron with prolonged mechanochemical activation, and the reaction of mineral phases over time, in MR3 mixes.

### 1. Introduction

Supplementary Cementitious Materials (SCMs) represent a promising avenue for mitigating the substantial carbon footprint in the built sector. Given the limited supply of widely used SCMs like ground granulated blast furnace slags (GGBFS) and fly ashes, there is a significant emphasis on exploring new sources to address this gap. The utilization of locally abundant natural pozzolans emerges as a viable alternative for replacing clinker [1,2]. For example, recent research on locally available clays, particularly those with a 1:1 type mineralogy, has shown great potential for replacing cement with activated clays [3,4]. When combined with limestone, calcined clays

\* Correspondence to: Chalmers University of Technology, Gothenburg 41296, Sweden.

E-mail address: [amrita.hazarika@chalmers.se](mailto:amrita.hazarika@chalmers.se) (A. Hazarika).

with at least 40% kaolinite content (LC3) have been found to enhance strength, refine pore structure, and improve durability [3–7]. This combination allows for up to 45% of the cement to be substituted. Additionally, LC3 binders have been demonstrated to reduce total CO<sub>2</sub> emissions by 38% compared to ordinary Portland cement (OPC). This promising research has led to pilot-scale implementations of LC3 binders in countries such as India, China, and Cuba [8].

However, most global clay resources contain less than 25% kaolinite and instead consist of a mix of less reactive 2:1 clay minerals and other non-clay minerals often considered impurities [9]. For instance, most clay resources in the Nordic [10–12] and South-East European regions [13], central Italy [14], as well as southern African regions such as Angola and Zambia [15], have no more than 25% kaolinite.

While research is underway to understand and utilize these lower-reactive clays in such regions [12,16–18], there is also significant potential to explore other available natural pozzolans in these areas. Of particular interest are natural pozzolans of volcanic origin, covering approximately 124 million hectares of the world's land surface. These pozzolans are found in regions experiencing a shortage of highly reactive clays, including Scandinavia, Africa, Southern Europe, Middle East Asia, Japan, North and South America, and New Zealand [1,19–24].

The volcanic materials (VMs), resulting from the pulverization of rocks or minerals during volcanic eruptions, manifest in various forms such as pumice, scoria, ashes, tuffs, hyaloclastites, palagonites, etc. [25]. Collectively referred to as pyroclastic or volcanic materials, they are derived from Andisols in regions with past or present volcanic activity. When combined with lime and water, they are capable of reacting with calcium hydroxide (CH), forming stable compounds with cementitious properties.

Volcanic materials have a rich historical significance as one of the earliest recorded building materials. They were extensively employed in ancient Rome, notably in the construction of the majestic Colosseum, which still stands as a remarkable testament to the strength and durability of cementitious materials. Additionally, volcanic glass found popularity in Mayan civilizations in the regions of central America and southern Mexico, where active volcanism prevails [26]. Despite the widespread availability of volcanic deposits worldwide, the advent and popularity of Ordinary Portland Cement (OPC) and subsequent industrial SCMs like fly ash led to a decline in the utilization and research of volcanic materials. This is noteworthy, considering the significant potential for construction

**Table 1**

Review of references of MCA parameters.

No.	Ref.	Minerals detected	Milling parameters used	Milling equipment	Observation
1	Pourghahramani and Azami 2015 [58]	Albite Oligoclase Orthoclase Quartz	Duration: 15, 30, and 45 min Speed: 400 rpm Ball to powder ratio: 24 Media: 15 balls, 20 mm dia, 490 g	Planetary mill	<ol style="list-style-type: none"> <li>Maximum surface areas were reached at 15 min for VM after which it declined.</li> <li>Amorphous material was produced upon grinding to 15, 30 and 45 min. Quantities of amorphous content is not measured.</li> <li>15 min ground VM showed the highest compressive strength when replacing cement by 10%.</li> </ol>
2	Djubo et al. 2016 [45]	Anorthite Feldspar Hematite Diopside sodian Forsterite syn Quartz	Duration: 30,60, 90 and 120 min Speed: unavailable Material to media ratio: 1:40 Media: Stainless steel balls of 12.5 mm	Eccentric vibratory mill	<ol style="list-style-type: none"> <li>For Anorthite, DOC decreases from 60% to 38% after 90 min MCA</li> <li>No relevant change in reactivity beyond 30 min of milling</li> <li>Decrease of D50 values till 60 min.</li> <li>Agglomeration and recrystallization beyond 90 min</li> </ol>
3	Almalkawi et al. 2017 [59]	Manitobite Melantrite	Duration: 3,4 h Speed: optimal rotational speed Material to media ratio: 10 Media: Steel ball of varying sizes (12,7 mm; 25,4 mm; 76,2 mm)	Ball mill	<ol style="list-style-type: none"> <li>MCA amorphized some constituents of raw pumice, however the quantities were not measured.</li> <li>Compared to thermal activation, MCA led to a growth of some crystalline structures like Melantrite.</li> </ol>
4	Szabo et al. 2023 [60]	Andesine Albite Cristobalite Microcline Smectite Quartz	Duration: 1,3,4,10 min Speed: rotor speed at 3 m/s and 5 m/s Filling ratio of grinding beads: 70 % Media: Grinding beads	Stirred media mill	<ol style="list-style-type: none"> <li>Amorphization increased by up to 7% from 1 to 10 min of MCA</li> <li>Lime adsorption and calorimetric results show that MCA increased reactivity of VMs.</li> <li>Specific surface areas continued to increase as a function of milling time up to 10 min.</li> </ol>
5	Tang et al. 2024 [46]	Albite Clinocllore Microcline Quartz	Duration: 15, 30, 45, 60 min Speed: 48 r/min Material to media ratio: 1:10 Media: 50 kg of steel balls of varying diameters	Horizontal planetary ball mill	<ol style="list-style-type: none"> <li>Decreased D50 with increased duration upto 60 min.</li> <li>Reduced crystallinity of quartz and feldspar was observed, but not measured</li> <li>45 min activated VMs showed the best strength when substituting OPC by 15%</li> </ol>

applications and the existence of numerous untapped volcanic deposits. These deposits offer mining with easier access and lower environmental impact than traditional clay quarrying, providing a superior cost-benefit ratio [19]. However, although abundant, only a small fraction of these deposits has been explored for use as potential SCMs.

In the Nordic region, the abundant availability of volcanic materials have catalyzed substantial interest in the industrial utilization of such resources within cement production [27,28]. Specifically for the region, volcanic ash from Iceland emerges as a promising candidate due to its vast availability, large reserves, and convenient transportation options via marine trade routes [29]. Studies aimed at further exploring and understanding this resource could greatly support its implementation.

In the past, numerous studies have emphasized the viability of incorporating volcanic materials as supplements to cement in the production of concrete [25,30,31]. This suitability is attributed to the pozzolanic nature of VMs, along with economic advantages, and environmental efficiency of reducing reliance on OPC. The extent to which VMs can replace traditional cement in concrete has been typically proposed to be around 20–35 % in standards [32,33]. Previous studies demonstrated that the replacements higher than 20 % generally led to lower compressive strength development and lower resistance to chloride ingress [34–37]. In another study by [38], it was shown that greater than 30 % substitution with volcanic ash led to increased porosity of the cementitious matrix.

Like clays, VMs are known to exhibit a wide range of minerals that vary in reactive silica and alumina contents. Table 1 shows some of the commonly detected minerals in pozzolans of volcanic origins across the world. However, there is a lack of research that highlights the role of mineralogy to the pozzolanic reactivity of VMs.

Nevertheless, multiple studies have tried different approaches to modify the reactivity of volcanic materials. Several studies have highlighted a relationship between reduced particle sizes of VMs and the enhanced pozzolanic activity [39–44]. As such, mechanical grinding or activation has been proposed as a promising route by past studies to promote the utilization of VMs in cement substitution [19,39,42,45,46]. According to reports, the reactivity of mechanically activated materials exceeds that of thermal or chemical activation methods, as there are modifications of physicochemical properties in the former [45]. Mechanical activation encompasses the initial breakdown of particles, subsequent elevation of internal and surface energy, increase of surface areas, and alterations in chemical structural order. This results in decreased degrees of crystallization, thereby increasing amorphization. Following this, there is aggregation of ground particles and recrystallization of activated phases [46–48]. Many researchers have termed this process as mechano-chemical activation (MCA) due to its combination of mechanical and chemical modifications. MCA has proven to be particularly effective in activating low-pozzolanic natural clays, demonstrating reduction of particle sizes, rise in specific surface areas, and increase in degrees of amorphization for clays [16,17,49,50]. In the case of VMs however, this technology is yet to be studied in depth. Although few studies have reported benefits of MCA for VMs, few challenges are yet to be addressed in this regard:

- i. There is a lack of uniformity and comprehensive information regarding the milling parameters employed, including grinding duration, speed (rpm), ball-to-powder ratio (B/P), feed size, among others. Although laboratory milling parameters are different than for industrial processing (it should be considered that explorations on laboratory scale should be implementable on industrial scale), yet to explore potentials of the materials on an industrial level, a comprehensive overview on noted parameters is essential. Table 1 presents a compilation of milling techniques and parameters utilized in some of the previous relevant investigations on MCA of various volcanic materials. However, there is a compelling need for further research to establish a correlation between milling parameters and their influence on variables that affect the reactivity of specific types of volcanic materials.
- ii. The physical and mineralogical properties of volcanic ashes vary based on the composition of their source magma, influencing their suitability as a cementitious material. In a previous study [25] conducted on 11 VMs sourced from various countries, significant variation in mineral content was observed across the samples. For instance, alumina content ranged from 19.6 % to 2.3 %, silica from 87.6 % to 46.6 %, iron oxide from 11.8 % to 0.4 %, CaO from 12.2 % to 0.2 %, MgO from 5.6 % to 0.2 %, and NaO from 6.5 % to 0.1 %. These differences highlight the diverse mineral compositions of VMs across different geographical regions. Owing to differences in diagenetic ages, weathering conditions, morphology, chemical compositions and other influencing factors of volcanic ash, notable variations in macroscopic performance might arise when substituting cement clinker [19,20,46]. As such, the activation parameters used for one type of VMs cannot directly be translated to another one with varied compositions and diagenetic history. This requires conducting additional studies on VMs with varied mineralogy, to leverage their abundant availability and potential as SCMs.
- iii. There is disparity in the evaluation of pozzolanic reactivity post activation treatments. The pozzolanic reactivity is a crucial requirement for the ash to be used as SCM in blended cement. Current studies on volcanic material (VM) activation often utilize two main types of pozzolanicity tests. The first type employs Portland cement as an activator (SAI: EN 13263, ASTM C1240, Frattini test: EN 196–5), while the second type uses lime (Chapelle, modified Chapelle test: NFP18–513, Indian lime reactivity test: IS 1727) [51,52]. These tests were primarily developed for SCMs with different mineralogical compositions and reaction kinetics, such as slag, fly ash, metakaolin, and silica fume. Consequently, these standardized tests are not directly applicable for analyzing VMs, which have significantly different mineralogy, particle sizes, surface areas, and morphologies.
- iv. Furthermore, previous research indicates that results from these two categories of tests often do not correlate. Lime-saturated tests may predict higher pozzolanic potential compared to the SAI or Frattini tests [53]. Additionally, these tests have been reported to be inconsistent for new SCMs [51,54] and show poor correlation with strength development [55]. An alternative approach is the R3 method, recently recommended in the RILEM TC 267-TRM report [56], which has been validated across a wide range of new SCMs. There is also a modified R3 test (MR3) specifically designed for low pozzolanic SCMs [57]. However, there is still a lack of research that quantifies the changes in reactivity levels of VM after activation using comprehensive pozzolanic tests such as R3 or MR3.

In the light of the unresolved challenges associated with the utilization of VMs, this study seeks to investigate the correlation between MCA parameters and the subsequent alterations in properties that influence the reactivity levels of four naturally sourced VMs. The four VMs are distinct in composition, age and geological formation, allowing for examination of varied effects of activation on corresponding physicochemical properties. The modifications in VM resulting from altered MCA parameters are analyzed and quantified in terms of their mineralogy, morphology, surface areas and reactivity levels.

The initial challenge in this investigation was to select the grinding parameters. Existing studies have showcased varied milling duration ranges, as outlined in Table 1. Typically, shorter durations ranging from 15 to 30 min, coupled with relatively higher speeds of up to 500 rpm, and a ball-to-powder ratio of approximately 25, have demonstrated favorable enhancements in amorphization and modification of physicochemical parameters for natural pozzolans such as VMs and heterogeneous clays [16,45,58]. In this study, a constant grinding speed of 500 rpm and a ball-to-powder ratio of 25 were chosen, with varying durations of mechanical chemical activation (MCA) until tangible effects on reactivity were observed. The primary objective in this study is to evaluate the effects of MCA on specific surface area, particle size distribution, morphology, and degree of amorphization, as well as to explore how changes in these parameters correlate with changes in reactivity. It should however be noted that achieving the optimum grinding parameters to achieve the maximum reactivity in the materials of focus is out of the scope of this study. In this study, the grinding parameters recommended in literature to achieve MCA is utilized [16,17,45].

The mineral compositions and the resultant changes owing to MCA on VMs have been studied with X-Ray diffractions (XRD). The morphology has been investigated with Scanning Electron Microscopy (SEM), particle size distributions were studied via laser diffraction, and specific surface areas through Brunauer-Emmett-Teller (BET) analyses of nitrogen sorption. Thereafter, these variables were linked to reactivity levels obtained from Modified R3 (MR3) tests [57].

## 2. Materials and methods

### 2.1. Raw materials

The volcanic materials utilized in this study were obtained from four locations in Iceland, sourced from volcanic deposits in the Southern regions such as Reykjanes, Mýrdalssandur, Búrfell and Ölfus. These materials, while locally sourced in Nordic region, share several mineralogical characteristics with volcanic materials found elsewhere, making the findings broadly applicable. They are hereby named VM 1, VM 2, VM 3 and VM 4 respectively. Fig. 1 shows the locations of the four VMs and Table A.1 in Appendix A describes the materials and their sources along with pictures of their as-received states.

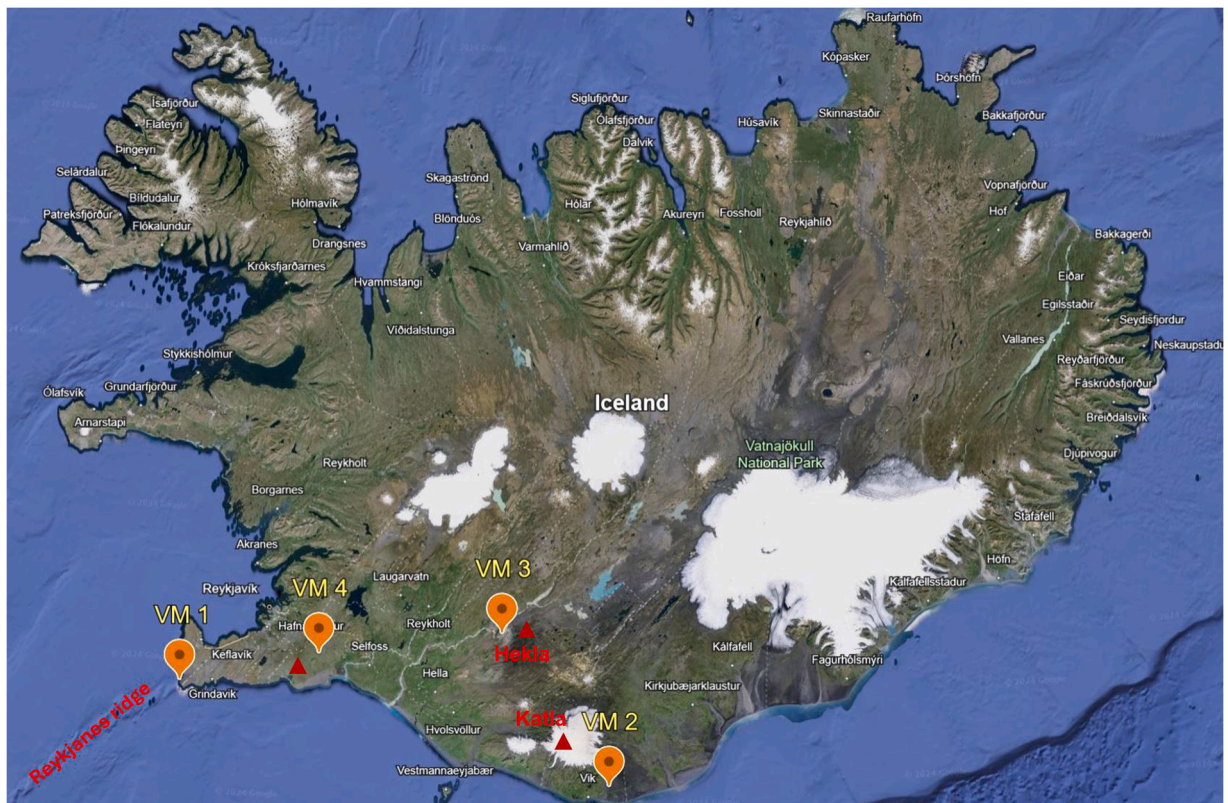


Fig. 1. Source locations of the four VMs in Iceland as depicted with orange location pins.

Table 2 presents the chemical compositions of the four VMs analyzed in this study. It can be observed that the silica and alumina contents, which are key contributors to pozzolanic reactivity, vary across the VMs. When compared to the VMs used in this study and other pozzolans examined in relevant literature, as shown in Fig. 2, VMs 3 and 4 exhibit notably higher silica content, indicating potential for higher reactivity among the tested VMs.

The volcanic rocks with pozzolanic potential are more concentrated in the southern part of Iceland and are predominantly identified as hyaloclastite and pumice [20,21]. In winter, the central and northern regions of Iceland face increased accessibility difficulties compared to the more accessible southern areas. Consequently, the study relies on materials extracted from two volcanic zones located in the southern part of the country.

Hyaloclastites are deposits resulting from explosive volcanic activity, formed through the fragmentation of magma either subglacially (under ice cover) or subaqueously (underwater) [61]. They primarily consist of basaltic glass, which is altered easily into another volcanic mineral called palagonite, along with secondary minerals. An earlier study found that basaltic and rhyolitic rocks possessed the lowest content of crystalline minerals among five volcanic materials that were classified based on silica content [62]. Hyaloclastites are currently getting recognized for their siliceous nature and have been identified to possess pozzolanic properties comparable to calcined clays [50]. Recent academic and industrial interests have surged in exploring the extensive potentials of using hyaloclastites as alternative SCMs [63–66]. Similarly, pumice is another volcanic formation that is abundantly available across volcanic belts [67–69]. Pumice has been previously studied and recognized as among the promising SCMs due to its reactivity upon sufficient particle grinding and its ability to contribute to strength gain [40,60,70,71]. The VMs used for this study belong to either of the two groups of hyaloclastite and pumice, as detailed in Table A.1.

## 2.2. Treatment and activation methods

The VMs initially acquired as agglomerates with varying sizes and excess moisture, underwent drying in a laboratory oven (LabRum Klimat) at 100 °C until a constant dry mass was achieved. Subsequently, larger chunks were reduced to smaller fragments through hammering and further ground using a planetary ball mill (Retsch PM 100) operating at 200 rpm for 5 min. The ball milling jar is stainless steel of 500 mL capacity. In this step, the feed includes 60 g of pozzolan material together with 30 stainless steel balls of 15 mm diameter.

Prior to the decision of mechanochemically activating the VMs, the reactivity of un-activated VMs was checked to establish a benchmark for comparison. To do this, VMs were ground at 200 rpm to make them pass through 75  $\mu\text{m}$  sieve before conducting a modified R3 (MR3) test as explained further in Section 2.3. However the reactivity levels achieved were in the range of 40–60 J/g SCM, which was below the threshold generally mentioned for reactivity tests. The reactivity results for the un-activated VMs are presented in the supplementary information.

The MCA was performed using the planetary ball mill, maintaining a fixed speed of 500 rpm, a ball-to-powder ratio of 25, and varying grinding durations of 5, 10, 15, and 20 min. The feed in this step includes 20 g of powder with 32 balls of 15 mm diameter. It is noteworthy that speeds exceeding 500 rpm could cause the balls to adhere to the container walls, reducing the milling efficiency. Simultaneously, prolonged grinding, while increasing energy consumption, could also elevate temperatures beyond 200 °C [48]. Considering insights from previous research on optimal grinding parameters for natural pozzolans and taking into account energy considerations, it was decided not to exceed a duration of 20 min to assess the activation effects on the physicochemical properties of the VMs.

## 2.3. Characterization methods

The chemical composition measurements were conducted with Inductively coupled plasma atomic emission spectroscopy (ICP-AES). For this method, a prepared sample of 0.1 g is added to lithium metaborate/lithium tetraborate flux, mixed well and fused in a furnace at 1000 °C. The resulting melt is then cooled and dissolved in 100 mL of 4 % nitric acid/2 % hydrochloric acid. This solution is then analysed by ICP-AES and the results are corrected for spectral inter-element interferences. Chemical composition is calculated from the determined elemental concentration. Loss on ignition (LOI) is then measured by TGA where 1 g of the prepared sample is weighed and placed in an oven at 1000 °C for one hour. Thereafter, the percent loss on ignition is calculated from the difference in weight before and after ignition. The negative values in LOI reflect possible oxidations and the standard error of the whole method is  $\pm 2$ , which explains why the total can vary between 98 % and 102 %.

The mineralogy of VMs was characterized by XRD which was conducted on BrukerD8 Discover in the 2 theta range 5–60° with step size: 0.02°, with time per step of 0.8 s. To assess changes in amorphous contents in the VMs with increasing grinding durations, a degree of crystallinity (DOC) was calculated. Thereafter, the degree of amorphization (DOA) were calculated based on the following formulae

**Table 2**  
Chemical composition (by weight percentage) of VMs.

Oxides wt%	SiO <sub>2</sub>	Al <sub>2</sub> O <sub>3</sub>	Fe <sub>2</sub> O <sub>3</sub>	CaO	MgO	Na <sub>2</sub> O	K <sub>2</sub> O	TiO <sub>2</sub>	MnO	P <sub>2</sub> O <sub>5</sub>	SrO	BaO	LOI	Total (%)
VM 1	43.80	14.60	13.25	11.95	7.44	2.09	0.15	1.50	0.21	0.13	0.01	0.01	– 0.51	99.14
VM 2	47.00	12.75	17.15	9.31	4.92	3.16	0.8	4.27	0.24	0.69	0.05	0.02	– 0.70	99.71
VM 3	65.60	14.90	7.70	3.62	0.83	4.73	1.98	0.65	0.19	0.19	0.02	0.06	1.44	101.98
VM 4	61.70	14.05	6.04	6.61	2.86	1.88	3.47	0.69	0.07	0.15	0.02	0.05	2.45	100.07

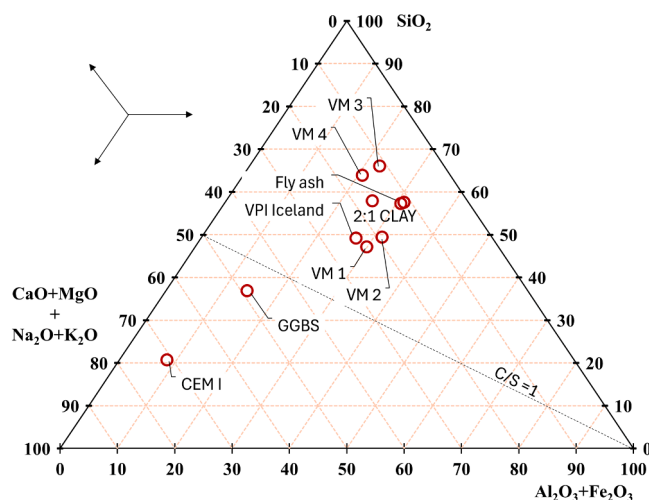


Fig. 2. Chemical composition range of the four VMs used in this study, in comparison to pozzolans reported in related literature [12,65,72].

[45,73–75]:

$$DOC(\%) = \frac{\text{Crystalline area}}{\text{Crystalline area} + \text{Amorphous area}} \cdot 100, \quad (1)$$

$$DOA(\%) = 1 - DOC(\%). \quad (2)$$

The crystalline area was determined by integrating the intensity of the crystalline peaks obtained in the XRD pattern, while the amorphous area was calculated as the integrated intensity of the region between the peak areas and a linear baseline [45,74,75]. The baseline was modeled as a linear function to approximate the amorphous contribution. The analysis was performed using the Peak Analyzer function of Origin software (OriginPro 2023), which allows for precise peak fitting and area integration. For peak fitting, Gaussian functions were employed to model the crystalline peaks. More information on the calculation is presented in the [Supplementary information](#).

It is acknowledged that this approach is semi-quantitative for determining the degree of amorphization (DOA). A standard deviation of  $\pm 3\%$  was observed across three repeat XRD measurements of the same sample, indicating the reproducibility of the method. Although a quantitative method like Rietveld refinement could offer more precise results for absolute amorphous values, yet, obtaining accurate quantitative measurements through this method is reportedly difficult [76,77]. This is especially true for heterogeneous pozzolans that exhibit variations in chemical compositions and structural order [78]. The principal objective of this part of the study is to examine the variations in individual amorphizations resulting from different grinding durations within the tested VMs. As a result, the DOC was calculated using the provided simple formula, enabling a comparative analysis of individual VMs rather than providing an absolute measure of their mineral quantification. This comparative analysis serves as a complementary parameter alongside other factors, enhancing the comprehensive understanding of the materials involved. For more accurate quantification endeavors, additional thorough investigations may be required in various research contexts.

The surface morphology of the activated VMs was observed by scanning electron microscopy (SEM) in secondary electron (SE) mode, using a FEI Quanta 200 FEG electron microscope. To prepare the samples for SEM, the VMs were first treated and activated as explained in [Section 2.2](#). Thereafter, about 1 mg of powdered samples were mounted on a SEM sample holder fitted with adhesive carbon conductive tape on the mounting surface. To ensure the representativeness of the samples studied with SEM, three different samples of the same kind were arbitrarily selected from a particular grinding batch of 20 g material. To minimize charging effects, the sample mounts were also fitted with copper tape on the sides. Images were obtained at an accelerating voltage of 20 kV at high vacuum mode.

To test particle size distribution, laser diffraction was conducted using Mastersizer 3000 (Malvern Panalytical) at a rotation rate of 2010 rpm. The dry powders were dispersed in water. The material was added in a beaker until the obscuration was around 10% after which the first measurement was conducted. Thereafter, the beaker was ultrasonicated for 60 s to break lumps, after which two consecutive measurements are taken. For specific surface area assessments, BET-SSA was conducted on TriStar 3000 with N<sub>2</sub> adsorption.

MR3 [57] was used to examine the reactivity levels of the activated VMs. For this purpose, isothermal calorimeter (I-Cal Ultra, Calmetrix) was used to study the heat release of MR3 mixes, at 50 °C for up to 10 days. For assessment of the hydrate phase and changes in the mineral peak intensities in the MR3 mix, paste samples were prepared for characterization through XRD. For this, samples of both 1 and 10 days MR3 were used. For the 1 day sample, a fresh mix of 10 g was prepared with the MR3 recipe. XRD was then conducted directly, using approximately 2 g paste. The remaining mix was put in the lab oven at 50 °C, for 10 days, in sealed containers. After 10 days, the pastes were first sawed into smaller pieces after which they were subjected to solvent exchange method with

isopropanol (2-propanol, ACS reagent > 99.5 % purity, Sigma Aldrich) for stopping the hydration [79]. The ground samples were then dried in a vacuum oven at 30 °C overnight. Afterwards they were sieved to obtain a particle size below 75  $\mu\text{m}$ . Thereafter, the XRD was conducted on BrukerD8 Discover in the 2 theta range 5–60° with step size: 0.02 °C with time per step of 0.8 s.

### 3. Results and discussions

#### 3.1. Mineralogy

Fig. 3 presents the XRD pattern of VMs. The most common phases that could be identified across the VMs are Anorthite, Albite, Andesine, Oligoclase and Olivine. Table 3 lists the CODs associated with the major minerals that could be characterized in the four VMs. A major Oligoclase peak around 2 theta of 22° is seen in VM 3 and 4 which has been reported earlier to be one of the primary constituents of materials from silicic volcanoes such as the ones in southern Iceland [21,80,81]. Oligoclase is recognized as a metastable and reactive mineral of silica found in volcanic rocks with an excess of silica [82]. In the context of using these materials as a potential cement replacements, previous research have indicated the high reactivity of oligoclase in the presence of lime, leading to the formation of calcium aluminosilicates or C-A-S-H as a reaction product [80].

By examining the oxide concentrations presented in Table 2, it is evident that VMs 3 and 4 exhibit higher SiO<sub>2</sub> levels compared to VMs 1 and 2. There are several silicate containing minerals reported for VMs (Anorthite, Albite, Andesine, Oligoclase, Olivine), however one specific mineral, Olivine, is known to have reactive silica [83,84] which is a phase detected in VMs 3 and 4, while it is not detected in VMs 1 and 2. Olivine is also known to be a highly reactive mineral that could be advantageous for facilitating higher reaction kinetics in these materials.

Fig. 4 illustrates the impact of progressively longer MCA durations on the mineralogy of VMs, accompanied by the calculated DOA using formula (2). The diffractograms reveal noticeable changes, such as peak widening or reduced peak intensities, with prolonged durations. Consequently, this alteration in peaks is reflected in the amorphous contents (DOA) with varying MCA durations, as depicted in Fig. 4. Longer MCA durations, particularly after 15 min, resulted in the potential formation of some new crystal phases. For identification of these peaks, additional measurements were conducted with a modified method file, on samples which are 15 and 20 min ground. The analyses of the additional measurements are provided in Fig. B.1 in Appendix B. The new crystal peaks were identified as Iron (43–44°, 50°, 74°, and 90°) and Magnetite (35°, 56°, and 62°). There are two possible theories why iron was detected likely after intensive grinding in VMs. The first could be due to wear of the steel ball mills at prolonged grinding times, as reported in [48]. The second reason, albeit less likely, could be because of deoxidation of Fe<sub>2</sub>O<sub>3</sub> to elemental iron (Fe) due to intensive mechanochemical milling, which is also a possibility and has been previously reported in [85–87]. The intense mechanical forces in a ball mill is known to break chemical bonds, which can drive reduction reactions, converting FeO into nano structured Fe, as grinding increases both heat and pressure locally, which can promote reduction. On the other hand, Magnetite can be formed due to the oxidation of iron oxides present in the VMs [39].

It was observed that longer grinding durations generally yielded in higher DOA. Increasing grinding durations from 5 to 20 min, shows an increase in DOA from 55 % to 72 % in VM 1, 67 % to 87 % in case of VM 2, and 75 % to 87 % in case of VM 4. In case of VM 3, while crystal peaks including those corresponding to Albite, Anorthite, Oligoclase and Olivine decreases or broaden with longer grinding durations, yet the amorphous contents did not vary widely. This is perhaps due to the simultaneous emergence of new phases that counterbalanced the overall amorphous contents.

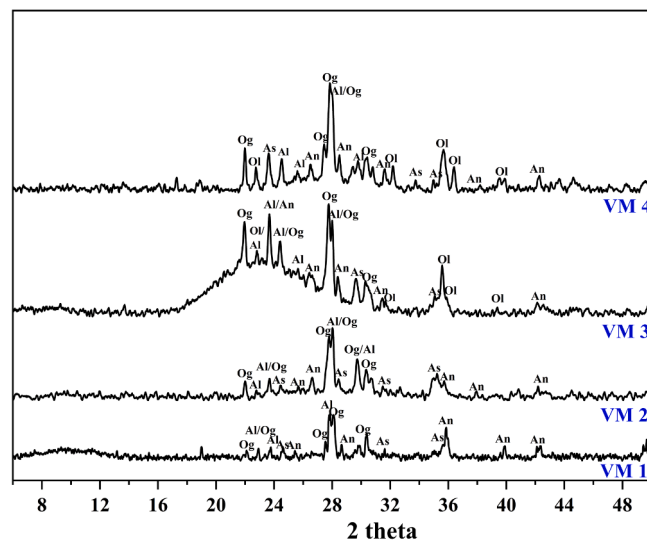
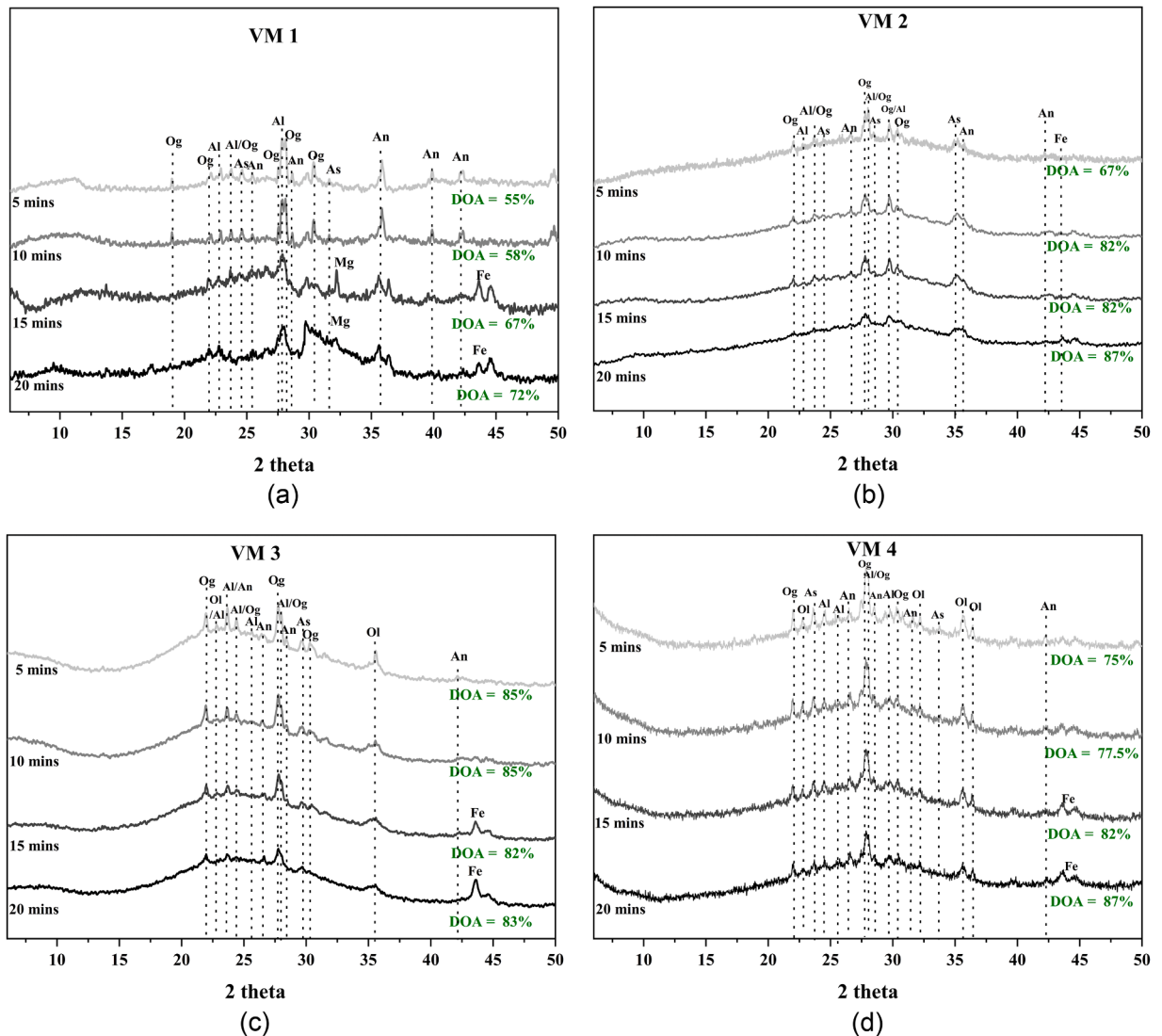


Fig. 3. Mineralogy of VMs identified through XRD. An = Anorthite, Al = Albite, As = Andesine, Og = Oligoclase, Ol = Olivine.



**Table 3**  
COD numbers of minerals characterized in the VMs.

Mineral	COD	VM
Albite (AlNaO8Si3)	9000526	All VMs
Anorthite (Al1.911Ca0.716Mn0.196Na0.045O8Si2.089)	9005309	VM 1, VM 2
	9000361	VM 3
	1000034	VM 4
Andesine (Al0.735Ca0.24Na0.26O4Si1.265)	9001031	All VMs
Oligoclase (Al1.277Ca0.277Na0.723O8Si2.723)	9011423	All VMs
Olivine (Fe0.2Mg1.8O4Si)	1533889	VM 3, VM 4



**Fig. 4.** XRD data showing the effect of varying MCA durations on the mineralogy of the four VMs. The degrees of amorphization (DOA) are also presented as calculated from the corresponding diffractograms. Al = Albite, An = Anorthite, As = Andesine, Og = Oligoclase, Ol = Olivine, Fe = Iron, Mg = Magnetite.

### 3.2. Morphology

Fig. C.1 (a–d) present the morphology of activated volcanic materials (VMs). A consistent trend is observed, wherein longer grinding durations seem to lead to the gradual formation of smaller, fragmented particles across all volcanic materials. Specifically, materials treated for only 10 min exhibit distinctly fragmented particles compared to 5 min ground particles, particularly evident in

VMs 2 and 3. In the case of VMs 1 and 4, it seems that fragments of small particles are attached to larger-sized particles at this stage. As the grinding duration increases, there is a noticeable emergence of more spherical particles. For some, the images do not reveal discernible further fragmentation of particles beyond a specific stage of grinding. Particularly for VMs 3 and 4, the particles resulting from 15 and 20 min of grinding do not appear significantly different from each other. However, the corresponding D50s presented in the following sections, indicate fragmentations occurring in these grinding stages as well.

### 3.3. Particle size distributions and specific surface areas

The PSD of the four activated VMs are presented in Fig. 5. In general, VMs demonstrate bi- or even multi-modal distributions across all the stages of grinding.

For VMs 1 and 2, the initial 5 min ground samples exhibit a prominent peak within the 50–1000  $\mu\text{m}$  range. As the grinding duration extends, this peak transforms into a wider hump, shifting towards smaller size ranges. The most significant alteration in this peak occurs in the samples milled for 20 min for both VMs. Concurrently, additional modes of distribution emerge in the finer size ranges, that becomes more evident with prolonged grinding beyond 5 min. This suggests an increased concentration of particles in these finer size categories with increased milling durations [88].

Examining the D50 results depicted in Fig. 6, it is evident that both VM 1 and VM 2 initially exhibited a higher D50 compared to the other VMs at the 5 min mark. However, this value consistently decreased with prolonged grinding, as also corroborated by the increased fragmentations observed across the different morphologies corresponding to the varying grind durations, presented in Fig. C.1. At 20 min, the D50 for VM 1 was 25  $\mu\text{m}$  compared to 75  $\mu\text{m}$  at 5 min, indicating a decrease of 67 %. For VM 2, the D50 at 5 min was 82  $\mu\text{m}$  which then decreased to 26  $\mu\text{m}$  (68 % lower) at 20 min.

Conversely, VM 3 and VM 4 initially displayed lower D50 values after 5 min of MCA compared to VMs 1 and 2. This is likely attributed to their inherently softer physical characteristics and consequent higher grindability [89]. For VM 3, the primary modal distribution was

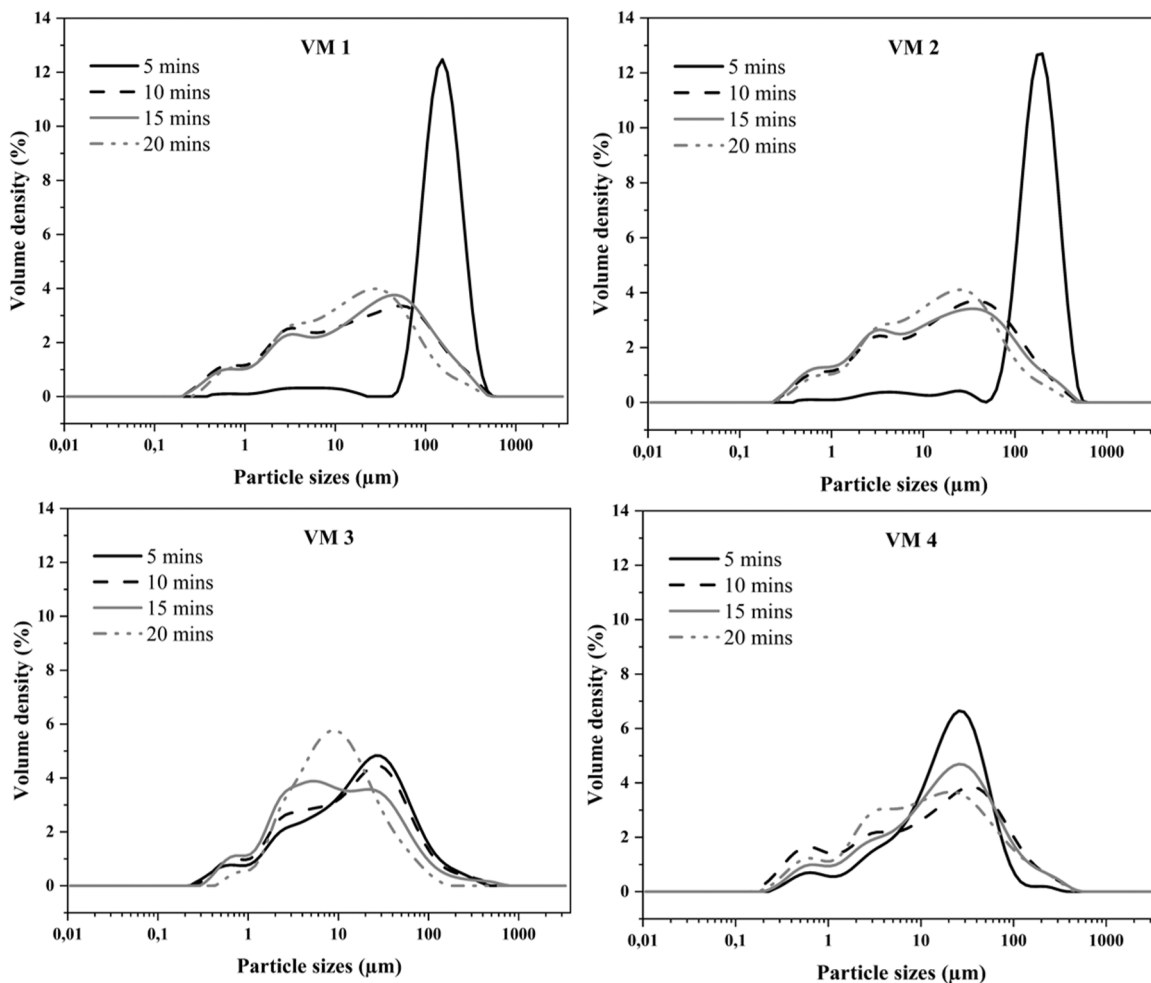


Fig. 5. PSD of activated VMs 1–4 respectively.

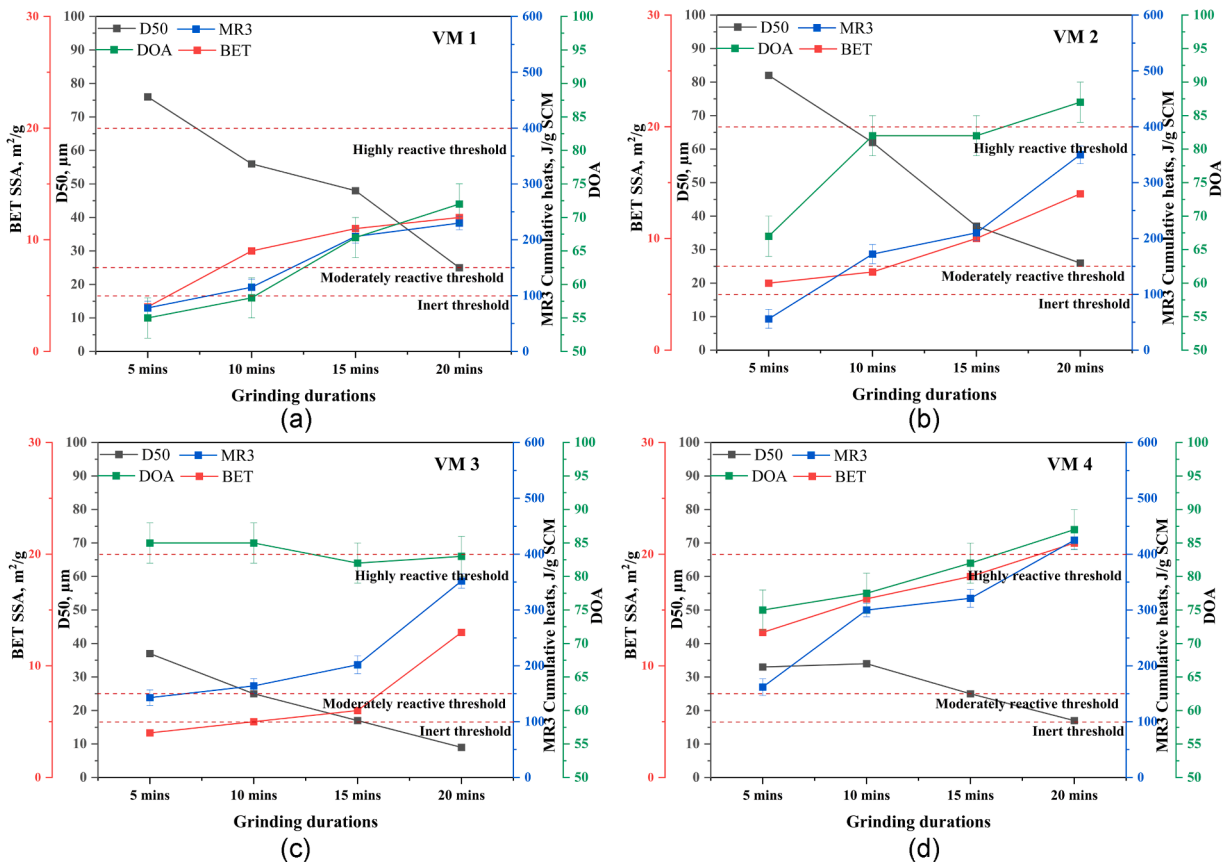


Fig. 6. Correlation between physical parameters (D50 and BET-SSA), DOA and reactivity (MR3) on account of increasing MCA durations.

concentrated in the 10–120 µm range at 5 min of MCA, while VM 4 exhibited a range of 6–100 µm. Transitioning from 10 to 15 min MCA in VM 3, a higher peak for 15 min is seen within the 1–10 µm range, accompanied by a smaller second shoulder in the 10–90 µm range. The D50 at 15 min decreased by 48.5–17 %, compared to the 5 min sample which had a D50 of 37 µm. Subsequent grinding to 20 min led to a singular modal distribution in the 1–90 µm range, with a corresponding D50 reduction of 76 % to 9 µm, compared to 5 min of MCA. In the case of VM 4, modal shifts were less pronounced in the PSD compared to other VMs. Nevertheless, the D50 still exhibited a reduction from 33 µm at 5 min to 17 µm at 20 min.

The specific surface areas, as determined by the BET-SSA method, exhibited noticeable changes with increasing grinding durations. The corresponding BET-SSA results, along with the D50 values and reactivity of the VMs assessed through MR3, are depicted in Fig. 6. Notably, a progressive rise in specific surface areas was observed in concurrence with diminishing particle sizes. For instance, VM 1 displayed a 23 % reduction (76 µm to 56 µm) in D50 from 5 to 10 min, correlating with a 125 % increase in surface areas (4–9 m<sup>2</sup>/g). Overall, when subjected to 20 min of MCA, VM 1 had a surface area of 12 m<sup>2</sup>/g compared to 4 m<sup>2</sup>/g at 5 min, exhibiting 200 % increase between the two grinding durations. Likewise, the surface area of VM 2 changed from 6 m<sup>2</sup>/g at 5 min to 14 m<sup>2</sup>/g at 20 min, demonstrating a 133 % increase, VM 3 showed a 225 % increase as it changed from 4 m<sup>2</sup>/g to 13 m<sup>2</sup>/g, and VM 4 changed from 13 m<sup>2</sup>/g to 21 m<sup>2</sup>/g or a 61.5 % increase in surface areas.

Distinct points were identified where shifts in surface area trends were particularly pronounced, notably in VMs 1, 2, and 3. VM 1 exhibited a significant turning point at 10 min of MCA, showcasing a 125 % rise in surface areas as it changed from 4 m<sup>2</sup>/g at 5 min to 9 m<sup>2</sup>/g at 10 min MCA. The PSDs and morphological images for 5 and 10 min MCA provide clear evidence of the formation of finer particles. In contrast, the morphology and PSDs during the subsequent transitions from 10 to 15 min and then from 15 to 20 min do not suggest substantial changes. Correspondingly, the increase in surface area was 22 % and 9 %, respectively.

VMs 2 and 3 experienced the points of maximum increase in surface areas following the shift from 15 to 20 min. At 20 min compared to 15 min of MCA, VM 2 exhibits a 40 % rise from 10 m<sup>2</sup>/g to 14 m<sup>2</sup>/g and VM 3 shows a substantial 117 % relative increase in surface areas from 6 m<sup>2</sup>/g to 13 m<sup>2</sup>/g. For VM 3, this sharp rise at 15 min MCA coincides with the observed formation of the new phase seen in the XRD.

In contrast, VM 4 exhibited a consistent increase of surface areas across all durations: 13 m<sup>2</sup>/g to 16 m<sup>2</sup>/g from 5 to 10 min, 16 m<sup>2</sup>/g to 18 m<sup>2</sup>/g from 10 to 15 min, and 18 m<sup>2</sup>/g to 21 m<sup>2</sup>/g from 15 to 20 min. The extent of observed changes in surface areas did not necessarily align with those in D50 values. The discrepancy might be ascribed to changes in morphologies, including alterations or fractures like the formation of mesopores. These alterations may not be easily detectable through SEM and may not necessarily indicate

a reduction in particle sizes; instead, they could contribute to an increase in specific surface areas [56,90]. As an example, in the case of VM 4, both the morphology in Fig. C.1 (d) and the PSDs in Fig. 5 did not indicate major changes beyond 10 min of grinding, but the specific surface areas continued to increase throughout.

### 3.4. Reactivity

In this study the reactivities of the four VMs are investigated in relation to three parameters: changes in mineralogy or degree of amorphizations (DOA), changes in particle sizes and specific surface areas occurring simultaneously with the activations. Fig. 6 present the reactivities of the VMs along with changes in in these parameters, corresponding to varying grinding durations. In Appendix A, further correlations between MR3 and BET-SSA, as well as MR3 and D50 are presented in Fig. D.1. The MR3 heat curves for the VMs are presented in Appendix D.

In general, it is observed that reactivities of the four VMs exhibit a linear increase with the duration of MCA. Three predictive thresholds from literature have been considered to categorize the VM reactivities obtained upon activations: inert below 100 J/g SCM, 150–400 J/g SCM signifying moderate reactivity and beyond 400 J/g SCM as highly reactive pozzolan [40,56,57,91,92].

Fig. 6 illustrate an observable correlation between the three parameters of MCA durations, D50, and BET-SSA, indicating a relationship with the obtained reactivities. Among the tested VMs, VM 4 demonstrated the capability to achieve even high-level reactivity beyond 400 J/g SCM when activated with 20 min MCA. Longer grinding durations result in lower D50 values and higher specific surface areas. The combined physical modifications induced by extended MCA on VM particles appear to contribute to higher reactivities for each individual VM. The generation of greater specific surface areas is known to facilitate faster reactivity, providing more sites for the nucleation of hydrate products [19,46].

Fig. 7 shows the ratios of 1–10 days heat release of the VMs ground to different time durations. It can be seen that the ratio overall increases with increasing grinding times. A higher 1–10 days heat release ratio signifies an increase in early reactions [93]. While a more detailed extrapolation of reaction kinetics would ideally include additional time points, this study focuses on correlating the effects of the grinding parameters with the reaction kinetics at the specific grinding durations. As prolonged grinding alters the particle size distribution, specific surface area, and amorphous content, the observed increase in heat release ratios is likely due to these changes.

From Figs. 6 and 7, it is observed that the combined effect of parameters such as specific surface area, D50 and DOA has a correlation to greater extent of reaction kinetics. For example, 20 min MCA for VMs 2 and 4 produces the highest surface areas and correspondingly the highest reaction kinetics. On the other hand, 5 min MCA for VMs 3 and 4 have comparatively higher reaction kinetics, which does not necessarily correlate with higher SSA, but more with the comparatively higher DOA and lower D50, potentially aiding in accelerating the reactions. At 10 min, VM 4 has the highest reaction kinetics, potentially because of the highest SSA among at this time point, among all VMs. From 10–15 min, VM 2 has the highest increase in reaction kinetics, possibly driven by the highest increase in SSA among all VMs, as well as the decrease in D50.

The degree of amorphous contents (DOA) in general correlates with the MR3 data in Fig. 6, yet there exists some anomalies such as in the case of VM 3 ground for 15 min, where regardless of the constant or slightly reduced DOA, the reactivity continues to increase, possibly due to the increase in the surface area. To understand which parameter out of amorphous content and specific surface areas govern the reactivity at a certain point, Fig. 8 is beneficial. This figure presents the reactivity per surface area, against the DOA corresponding to different grinding durations. Combining Figs. 6 and 8 it is seen that for VM 1, 10 min MCA had a higher impact on

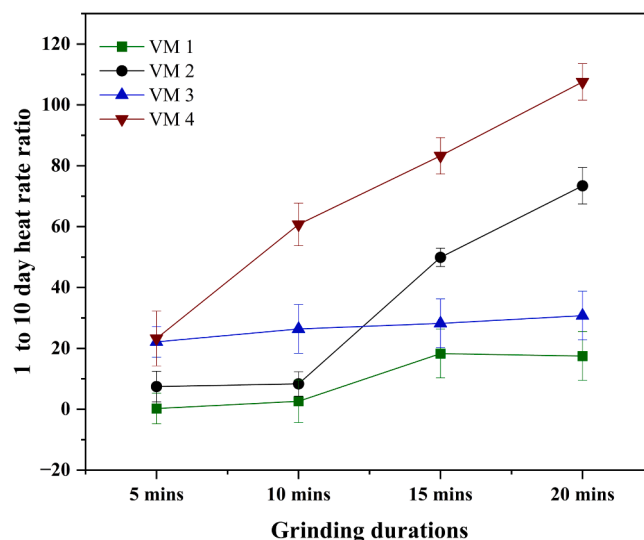


Fig. 7. Variation of heat rate ratios between the VMs ground to varying time durations.

surface area than on the DOA, while in the 15 min ground sample, the increase in BET-SSA was lower than the increase in DOA. Similar observations can be made for the other VMs which, at different points, exhibit varying levels of contribution from DOA and BET-SSA towards reactivity. Therefore, reactivity can be regarded as combination of both these parameters.

It is noted that the maximum increase of DOA was observed for VM 2, which had  $67\% \pm 3$  at 5 min and  $87\% \pm 3$  at 20 min MCA, which also correlated to the highest increase in reactivity over the same timeline for the VM. One possible explanation for the varied impacts of MCA on the VMs is the differing levels of crystallinity among the materials. Crystallinity significantly influences hardness, as materials with higher crystalline phases tend to exhibit greater resistance to fracture or grinding. This behavior is attributed to their denser and more orderly packed microstructure [94,95]. For instance, VM 1, which has a higher proportion of crystalline phases compared to the other three VMs, may have been more resistant to reductions in D50 and SSA. This resistance could explain why MCA was less effective for VM 1 than for VM 2, where the lower crystallinity might have facilitated a more pronounced response. Consequently, crystallinity differences, in addition to variations in reactive mineral phases, may account for the limited effectiveness of MCA on VM 1. Another possible explanation could be differences in the composition of amorphous phases present across the VMs. While not examined in the current study, the quantity and composition of these amorphous phases likely influence reactivity.

On average, it was observed that 15 min of MCA was necessary for VMs 1–3 to attain moderate levels of reactivity, while VM 4 reached moderate reactivity with only 5 min of MCA. For VM 4, the D50 at 5 min was the lowest among the tested VMs, accompanied by the highest BET specific surface area at this stage, indicating that the material had already undergone particle fragmentations with only 5 min of grinding. Notably, although the starting material for VM 4 was coarser in size than that of VMs 1 and 2, it was more easily disintegrated into smaller particles, highlighting its higher grindability. Additionally, VM 4 exhibited the highest BET-SSA after 20 min of MCA, along with the highest MR3 at this stage, surpassing all other VMs.

Fig. 9(a) and (c) present the X-ray diffractograms of the MR3 samples taken after 10 days, containing VMs ground with 5 min and 20 min MCA respectively. The presence of Portlandite (CH) and AFm (Hemi- and Mono-carbonates) is consistently observed across all samples. The CH was added as a reactant with the mix with a VM to CH ratio of 1:3. To assess the consumption of CH, the peak intensities corresponding to  $18^\circ 2$  theta are selected for both 5 and 20 min ground VMs, as illustrated in Fig. 9(b) and (d) respectively. It is evident that at 5 min, CH consumption is comparable among VMs 1, 2, and 3, while VM 4 exhibits a lower peak intensity, indicating higher CH consumption. Conversely, at 20 min, variations in CH peak intensities are more pronounced across the VMs. When considered alongside Fig. 6, which represents the cumulative heat evolution levels from MR3 tests, it becomes apparent that peak intensities, or CH consumption levels, align with the observed reactivity levels. At 20 min, VM 4 demonstrates the highest CH consumption, while VM 1 exhibits the lowest. Fig. F.1 presented in Appendix F further shows the individual curves for the VMs, at a reduced scale of intensity, in which both hydrates and mineral changes are visible after 10 days of MR3 in the 5 min and 20 min MCA samples.

To understand the reaction of mineral phases, the diffractograms presented Fig. 10 could be beneficial. This figure presents the mineral crystals that could be distinguished in the 1st and 10th day's MR3 mix of the four VMs. All the VMs used were ground with 20 min MCA. The colored lines represent day 1 and the lighter gray lines represent day 10 diffractograms.

The figure presents the main mineral peaks that stand out in the otherwise noisy diffractograms, which is potentially a result of the matrix consisting of VM to CH ratio of 1:3 and the overlapping of several diffraction peaks. In particular, the following mineral peaks can be identified according to the COD databases provided earlier in Section 3.1: Albite (with 2 thetas corresponding to  $21.9^\circ$ ,  $28^\circ$ ), Anorthite (with 2 thetas corresponding to  $12.7^\circ$ ,  $13.3^\circ$ ,  $15.01^\circ$ ,  $19.95^\circ$ ,  $27.41^\circ$ ,  $35.8^\circ$ ), Andesine (with 2 thetas corresponding to  $21.95^\circ$ ,  $35.83^\circ$ ,  $42.17^\circ$ ), Olivine (with 2 thetas corresponding to  $35.6^\circ$ ,  $36^\circ$ ,  $51.98^\circ$ ,  $57.21^\circ$ ) and Oligoclase (with 2 thetas corresponding to  $21.9^\circ$ ,  $24.56^\circ$ ,  $28.04^\circ$ ,  $30.35^\circ$ ,  $43.05^\circ$ ).

It was observed that compared to the 1st day, the intensities of the mineral peaks across all VMs, were much reduced on the mix

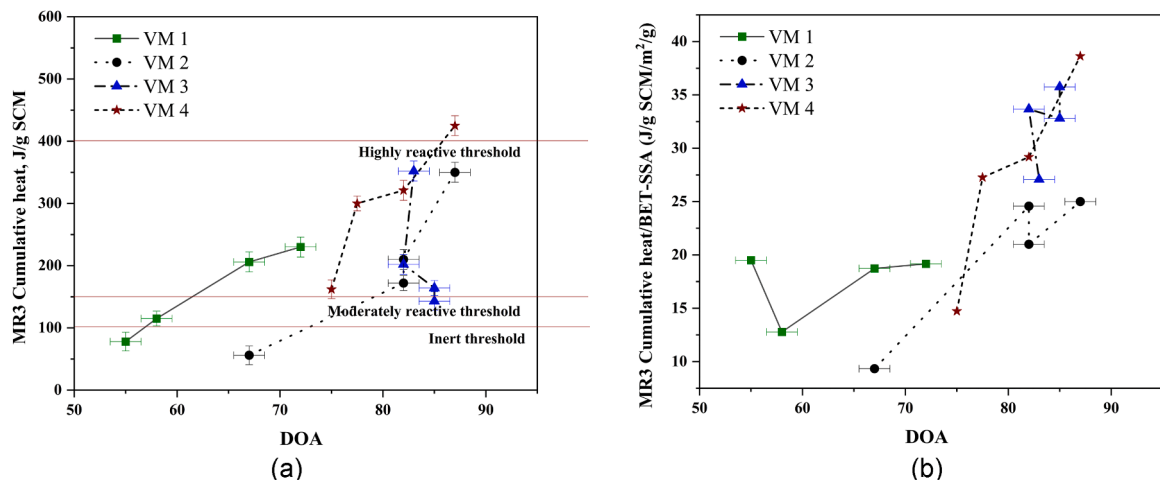
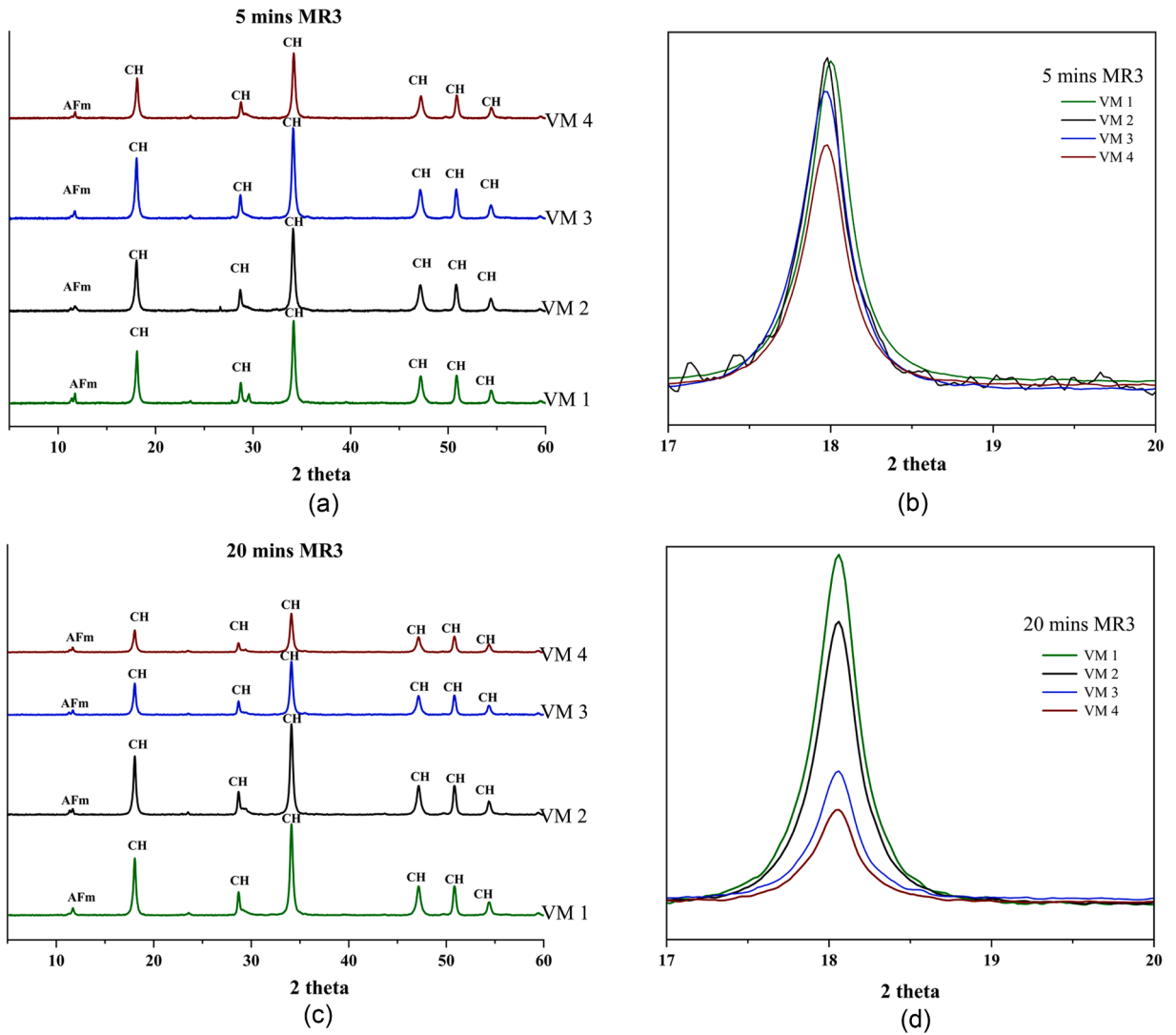


Fig. 8. Contribution of DOA on the reactivity. Correlation between MR3 and DOA. (b) Effect of DOA in contrast to BET-SSA.



**Fig. 9.** Hydrates of the 10 days MCA samples containing 5 min (a) and 20 min (c) ground VMs. Alongside are the variations of CH consumptions observed in the CH peak at 18°, in 5 min (b) and 20 min (d) ground samples. AFm = Mono and Hemi-carbonates, CH = Calcium Hydroxide/Portlandite.

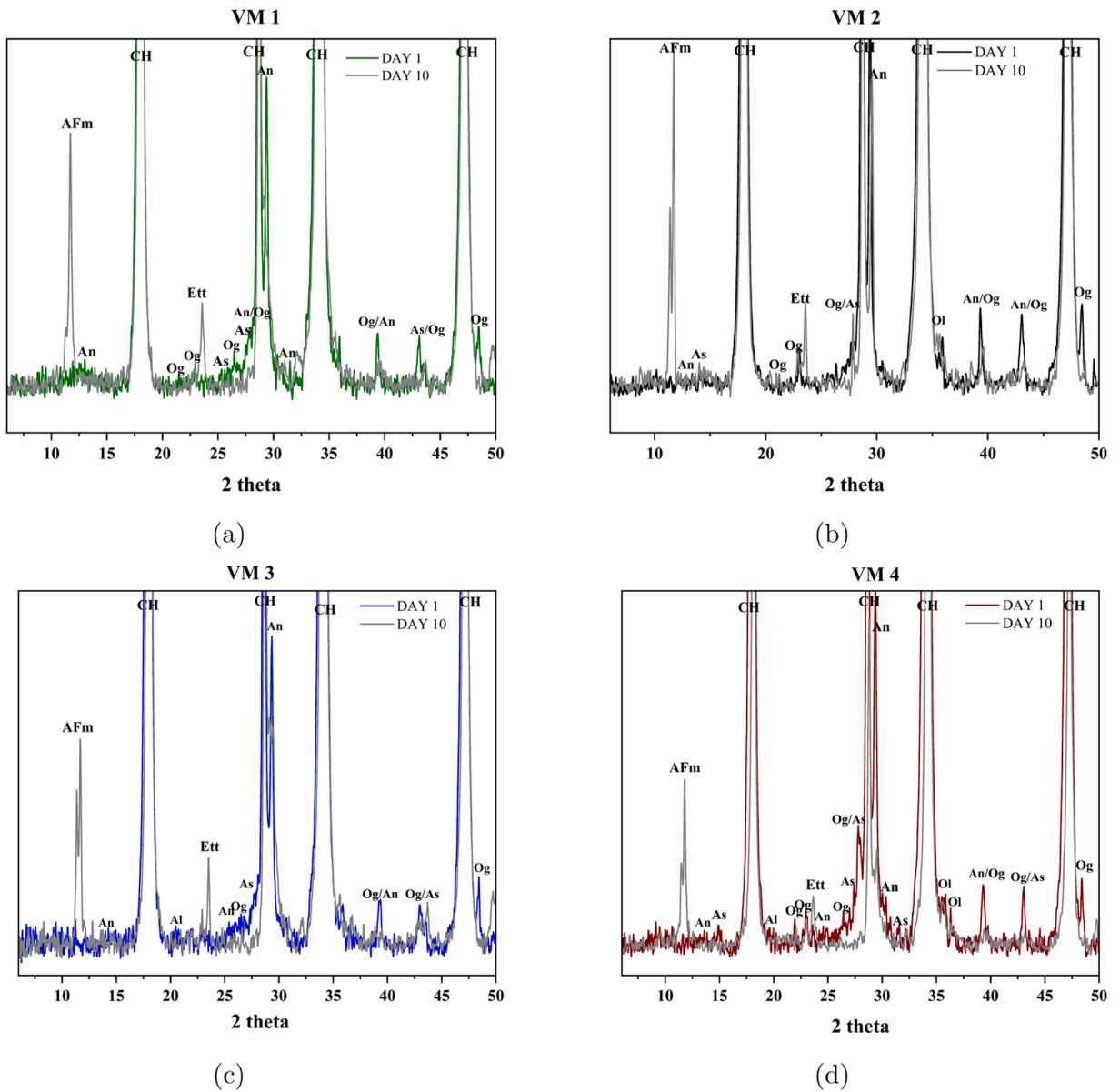


Fig. 10. (a–d): VM crystal peaks as distinguished in day 1 of MR3 mix, compared to day 10 of the same mix. The VMs were ground with 20 min MCA. Al = Albite, An = Anorthite, As = Andesine, Og = Oligoclase, Ol = Olivine.

corresponding to day 10. This implies the potential reaction of these mineral phases over the period. Among the VMs, it could be noticed that in day 1, the mineral peaks such as Albite, Oligoclase, Anorthite and Andesine in VM 3 shows higher intensities than for VM 2. On the same samples at day 10, the corresponding peaks appear diminished. The reaction of these phases indicate mineralogical contribution towards the reactivity, in addition to improved physical attributes such as specific surface areas.

The minerals detected in the VMs majorly belong to the Feldspar group (except Olivine). Feldspars are known to be relatively less reactive than other reactive silica minerals typical of volcanic materials, such as opal or volcanic glass. However, intensive milling conducted through the MCA process is known to increase dissolution and phase transformations in Feldspar minerals, which forms unstable phases [96,97]. Increase in dissolution has been correlated previously to an increase in reactivity of Feldspar minerals [96]. The diminished mineral peaks of 20 min ground samples at 10 days, seen in Fig. 10, further indicates the reactivity of activated Feldspar minerals.

#### 4. Conclusion

Volcanic materials (VMs) are yet underutilized natural pozzolans that hold significant potential for replacing low clinker cements. However, they face challenges in application due to their lower reactivity. Mechanochemical activation (MCA) has emerged as a beneficial approach for modifying the physicochemical properties of VMs to enhance their reactivities; however, questions remain regarding the diverse milling parameters used for MCA and the lack of a comprehensive investigation linking the parameters affected by activation methods with VM reactivity levels.

The current study focuses on four VMs sourced from active volcanic regions in Iceland: VM 1 from Reykjanes Ridge, VM 2 from Katla central volcano, VM 3 from Mt. Hekla, and VM 4 from Mt. Litla-Sandfell. Each differed in terms of diagenetic ages, chemical compositions, and physical attributes like surface hardness and grindability. The study aimed to assess the physicochemical characteristics of the four VMs susceptible to modification by MCA, including particle size distributions (PSD), specific surface areas, and amorphous contents (DOA). Consequently, the relationships between these alterations and reactivity levels were studied using conventional reactivity thresholds. Moreover, some insights into the contribution of mineral phases towards reactivity could be analysed.

The following are the primary conclusions from the assessments:

- i. Among the four different durations of 5, 10, 15 and 20 min, longer periods of MCA were found to induce greater particle fragmentations, resulting in finer particle size distributions and increased specific surface areas. Across all the four VMs, from 5 min to 20 min MCA, the specific surface area increased by  $8 \text{ m}^2/\text{g} \pm 1$ . The increase in surface area at longer grinding durations correlated to increases in reaction kinetics of activated samples.
- ii. XRD analysis of activated samples revealed that longer milling times generally increased DOA. The maximum increase of DOA was observed for VM 2, which had  $67 \% \pm 3$  at 5 min and  $87 \pm 3$  at 20 min MCA, which also correlated to the highest increase in reactivity over the same timeline for the VM. At varying durations across the grinding regime, the contribution of both specific surface area and DOA, mutually correlated to an increase in the MR3 reactivity.
- iii. Mixes with 20 min ground VMs demonstrate higher portlandite consumption than the corresponding 5 min ground sample mixes. At the same time, mineral phases of 20 min ground samples demonstrated reduced intensities from 1 to 10 days, indicating the possible contribution enhancing the reaction kinetics and contributing towards higher reactivity.

#### CRedit authorship contribution statement

**Amrita Hazarika:** Conceptualization, Writing original draft, Review & Editing, Methodology, Investigation, Formal analysis, Data curation. **Liming Huang:** Writing – review & editing, Supervision, Methodology. **Sigurdur Erlingsson:** Writing – review & editing, Resources. **Klaartje de Weerd:** Writing – review & editing, Supervision, Methodology. **Ingemar Löfgren:** Writing – review & editing. **Sahar Iftikhar:** Formal analysis. **Arezou Babaahmadi:** Conceptualization, Writing – review & editing, Supervision, Methodology, Funding acquisition, Formal analysis.

#### Declaration of Competing Interest

The authors declare that they have no known competing financial interests or personal relationships that could have appeared to influence the work reported in this paper.



## Data availability

Data will be made available on request.

## Acknowledgements

The study has been financed by several organisations. The authors acknowledge the grant offered by FORMAS, the Swedish research council, for the project: *New era for cement replacement materials: Importance of service life design* (NewDurCem with Grant no.: FR-2020/0008), and Family Thomas Foundation for project: *Evolution of pozzolan incorporated concrete: resistance to carbonation* (Carbo-crete). This work is also partially funded by Vinnova (Sweden's Innovation Agency), and is connected to the project: *Towards a climate neutral and resource efficient soil stabilization additive* with Grant no.: 2021-01053. The authors sincerely thank the contributions of the following personnel and faculty: Jose Everton at VTI (Swedish National Road and Transport Research Institute, Linköping) for laser diffraction measurements, Jennie Isaksson and faculty at ALS Geochemistry Lab for ICP-MS measurements, Michal Strach at CMAL (Chalmers Materials Analyses Lab) for generous assistance with XRD, as well as Stefan Gustafsson for helping with SEM, our student assistants Mohammad Tahmasebi and Suriyaprakash Saravanan, at Chalmers Building Materials Lab for helping with material preparations, and Luping Tang for his assistance and co-supervision.

## Declaration of competing interest

None.

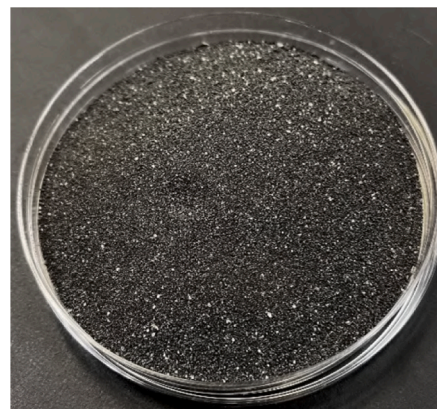
## Appendix A. Description of sources and images of the four volcanic materials

**Table A.1**

Description and images of VMs.

VM 1

<b>Location</b>	Reykjanes, 63.817803, – 22.727972
<b>Source</b>	Submarine eruption on the Reykjanes Ridge
<b>Time of origin</b>	1226
<b>Description</b>	A granular basaltic tephra sample, characterized by its dark grey to black color, was collected at a depth of 0.5 m from the surface (within layer R-9) along the shoreline at the tip of the Reykjanes peninsula. This location marks the convergence point of the Reykjanes Ridge with the landmass. The tephra is a product of a submarine phreatic eruption believed to have occurred in the 13th century at the boundary where the Reykjanes Ridge intersects with the westernmost volcanic system among the four sub-parallel volcanic systems present on the Reykjanes peninsula, known as the Reykjanes volcanic system [98].





VM 2

<b>Location</b>	Mýrdalssandur, 63.445639, – 18.805458
<b>Source</b>	Katla central volcano
<b>Time of origin</b>	1918

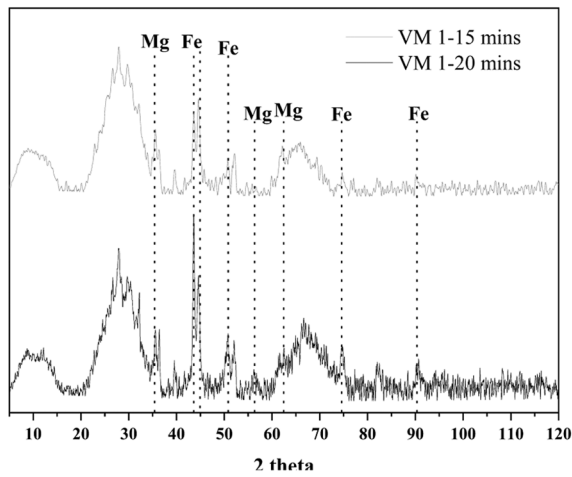
(continued on next page)

Table A.1 (continued)

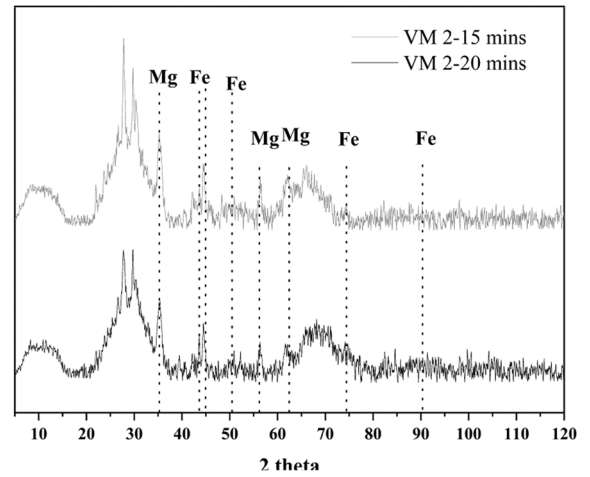
VM 1		
<b>Description</b>	The last recorded eruption of the Katla sub-glacial central volcano beneath the Mýrdalsjökull glacier dates back to 1918. This event was accompanied by a swift and intense meltwater flood known as a glacier outburst or “jökulhlaup.” The basaltic magma interacting with the ice triggered a rapid flow of water and debris, depositing a significant amount of tephra across the vast Mýrdalssandur outwash plain located southeast of the volcano [99]. The referenced sample was obtained from the material resulting from the 1918 eruption, extracted at a depth of approximately 1 m within the outburst deposits.	
<b>VM 3</b>		
<b>Location</b>	Open tephra quarry by Burfell, 64.059683, – 19.785778	
<b>Source</b>	Mt. Hekla central volcano	
<b>Time of origin</b>	2900 BP (before present)	
<b>Description</b>	Mt. Hekla, positioned along the western edge of Iceland’s Southern Eastern Volcanic Zone, is renowned for its mixed eruptions, combining tephra and lava of varying compositions, ranging from silicic to intermediate, including basalt, basaltic andesite, dacite, and rhyolite [100–102]. The eruption approximately 2900 years ago dispersed a significant amount of light-colored or whitish airborne tephra across over 80 % of Iceland, forming a distinct layer known as H-3. Thick accumulations of H-3 can be found just a few kilometers north of the volcano, notably within an open tephra (pumice) quarry, where the referenced sample was collected from a shallow depth.	
<b>VM 4</b>		
<b>Location</b>	Litla-Sandfell, Olfus, 63.958268, – 21.459016	
<b>Source</b>	Mt. Litla-Sandfell	
<b>Time of origin</b>	The Weichselian glacial, the last glacial event between 110 and 11.7 thousand years ago.	
<b>Description</b>	Mt. Litla-Sandfell, a small mountain, emerged through a subglacial fissure eruption during the Weichselian period. Situated within the southern sector of the easternmost volcanic system among the four volcanic systems dotting the Reykjanes Peninsula [103], it bears witness to Iceland’s dynamic geological history. The sample procured from this mountain consists of lightly lithified tuff of basaltic origin, exhibiting signs of alteration, notably palagonitization, resulting in a distinct yellowish-brown color.	

## Appendix B. Phase identification

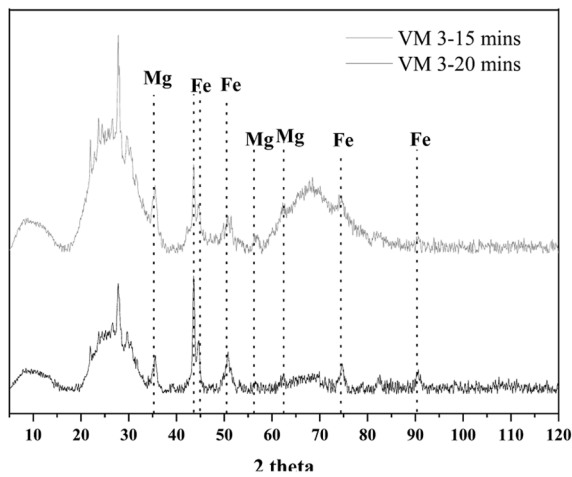
The following figures present the XRD peaks obtained on 15 and 20 min MCA samples. In particular, the peaks and mineralogy of the new phases developed in the VMs after this grinding timeline, has been focussed. The rest of the mineralogy has been presented in Section 3.1.



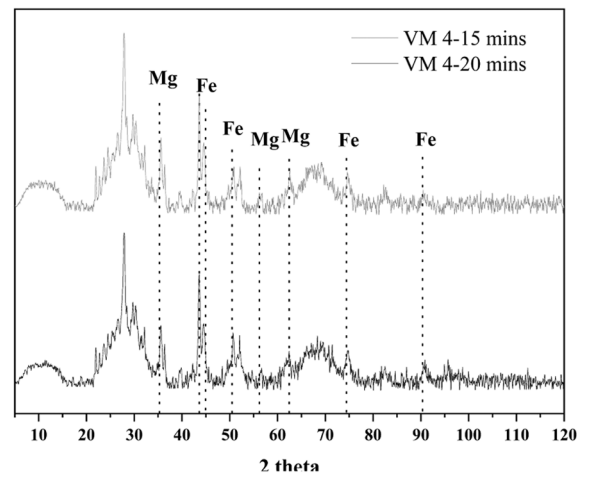
(a) VM 1



(b) VM 2



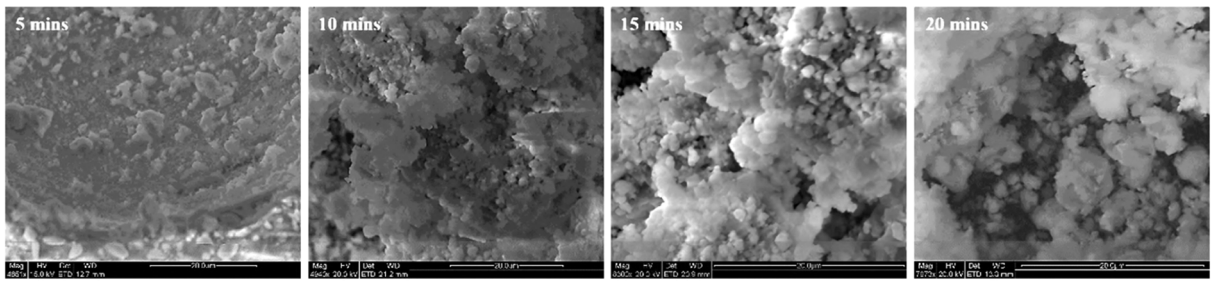
(c) VM 3



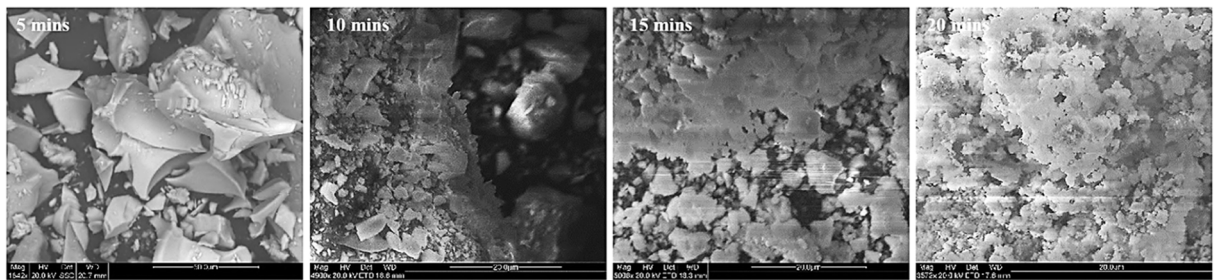
(d) VM 4

**Fig. B.1.** New crystalline phases formed at 15 and 20 min MCA in the VMs. Mg = Magnetite ( $\text{Fe}_2\text{O}_4$ ) with COD: 9005813, Fe = Iron with COD:9008469, 9000657.

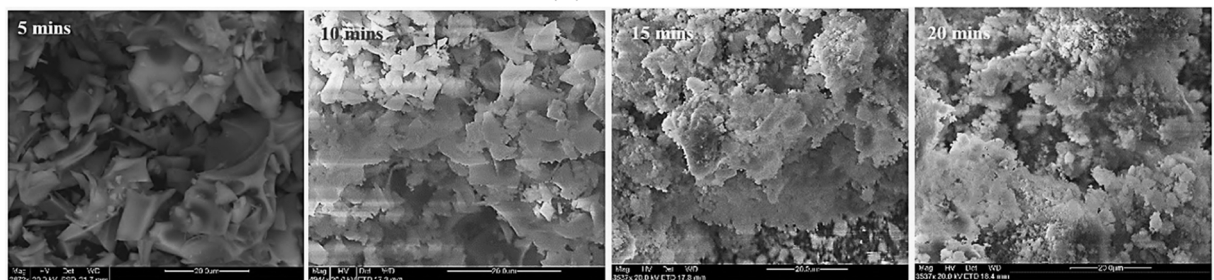
Appendix C. Morphology



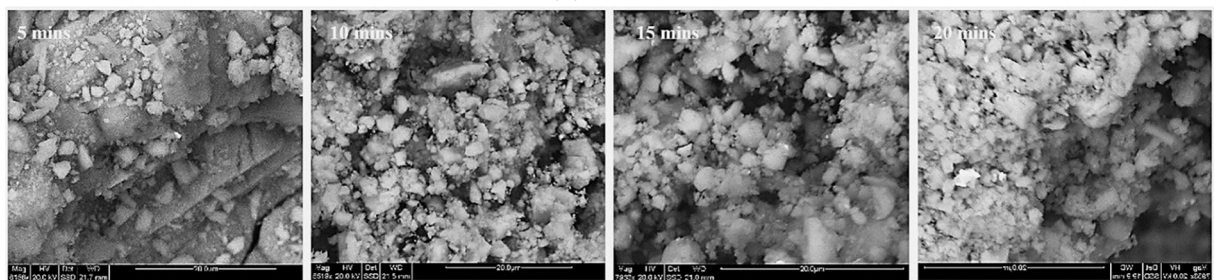
(a) VM 1



(b) VM 2



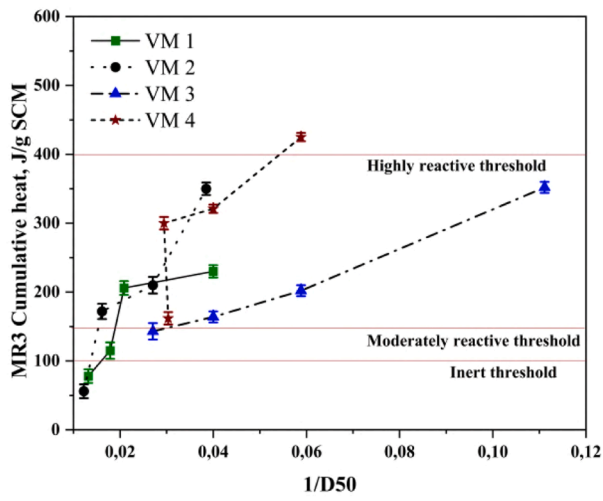
(c) VM 3



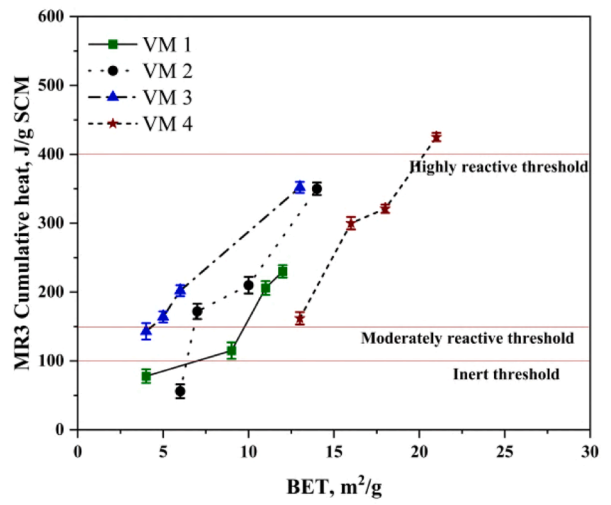
(d) VM 4

Fig. C.1. Morphology of VMs under progressive MCA treatments analysed with SEM-SE. The scale of images is 20 µm.

Appendix D. Correlations between MR3 and physicochemical properties



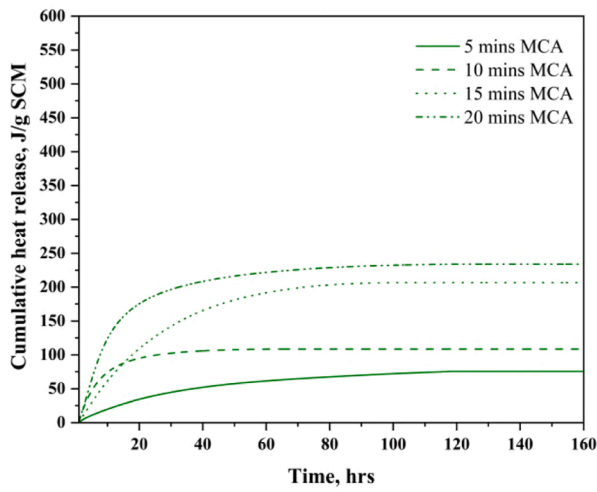
(a) MR3 and 1/D50



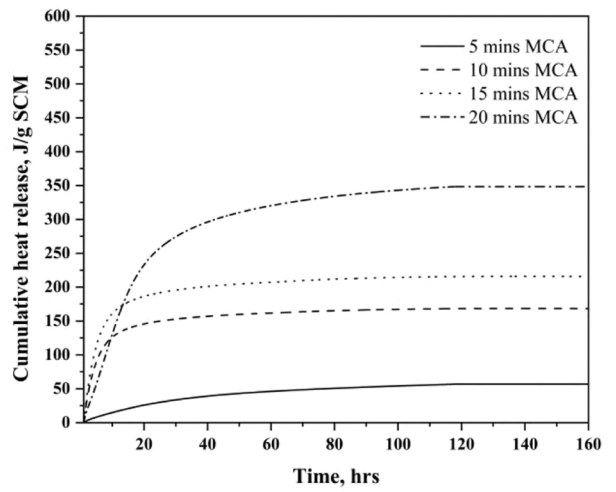
(b) MR3 and BET-SSA

Fig. D.1. Correlation between the reactivity (MR3) of the four VMs and (a) Particle sizes (1/D50), (b) specific surface areas (BET-SSA).

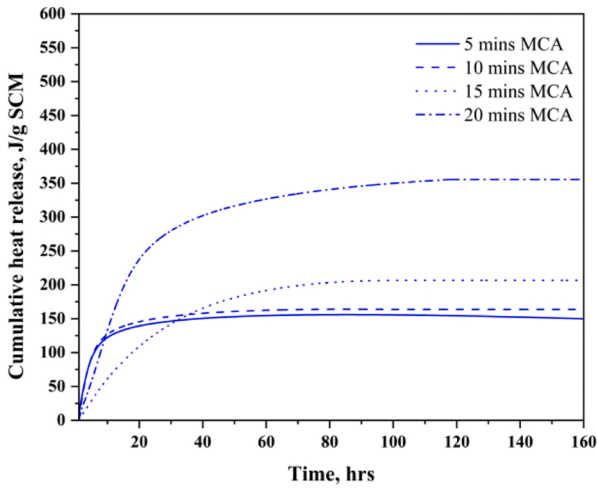
**Appendix E. MR3 Reactivity heat curves**



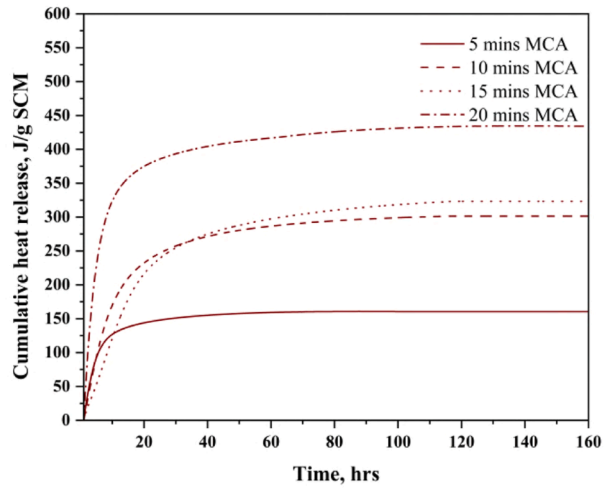
(a) VM 1



(b) VM 2



(c) VM 3



(d) VM 4

**Fig. E.1.** Cumulative heat curves from MR3 isothermal calorimetry test, conducted with VMs.

**Appendix F. Development of hydrates and crystal phases after MR3**

This section presents the individual graphs of hydrates formed during MR3 reaction, together with the changes in main mineral phases. The age of all samples here are 10 days.

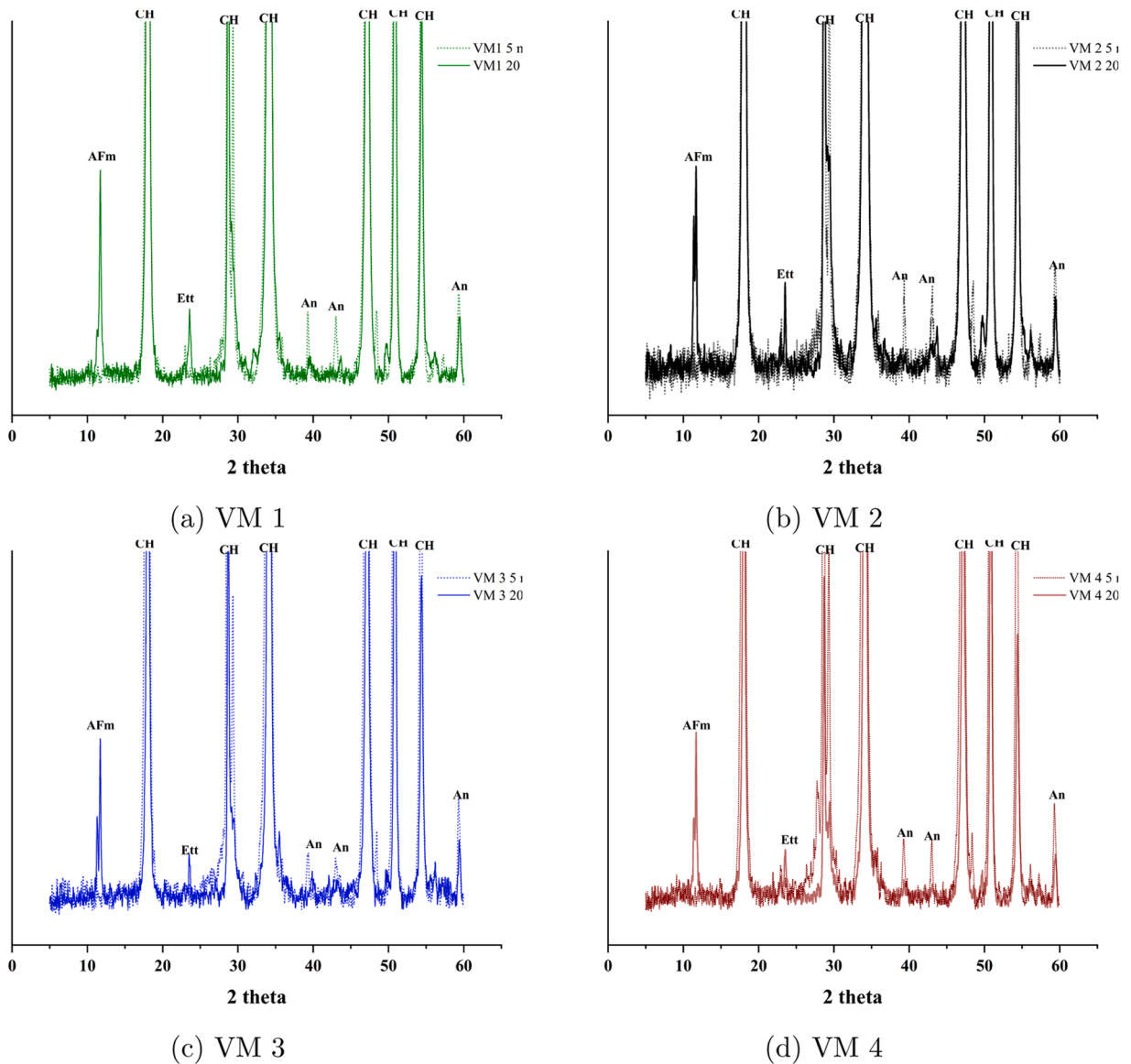


Fig. F.1. Hydrates and mineral crystals as identified after MR3 test for 10 days, on 5 min and 15 min MCA samples. The scale of the plots are adjusted to present the intensities of both hydrates and mineral crystals.

## Appendix G. Supporting information

Supplementary data associated with this article can be found in the online version at [doi:10.1016/j.cscm.2024.e04096](https://doi.org/10.1016/j.cscm.2024.e04096).

## References

- [1] R.A. Robayo-Salazar, et al., Study of synergy between a natural volcanic pozzolan and a granulated blast furnace slag in the production of geopolymeric pastes and mortars, *Constr. Build. Mater.* 157 (2017) 151–160, <https://doi.org/10.1016/J.CONBUILDMAT.2017.09.092>.
- [2] M. Najimi, et al., Comparative study of alkali-activated natural pozzolan and fly ash mortars, *J. Mater. Civ. Eng.* 30 (6) (2018) 1–9, [https://doi.org/10.1061/\(asce\)mt.1943-5533.0002306](https://doi.org/10.1061/(asce)mt.1943-5533.0002306).
- [3] K.L. Scrivener, Options for the future of cement, *Indian Concr. J.* 88 (7) (2014) 11–21.
- [4] M. Sharma, et al., Limestone calcined clay cement and concrete: a state-of-the-art review, *Cem. Concr. Res.* 149 (August) (2021) 106564, <https://doi.org/10.1016/j.cemconres.2021.106564>.
- [5] H. Maraghechi, et al., Performance of limestone calcined clay cement (LC 3) with various kaolinite contents with respect to chloride transport, *Mater. Struct.* 51 (5) (2019) 1–17, <https://doi.org/10.1617/s11527-018-1255-3>.

- [6] Y. Dhandapani, Mechanical properties and durability performance of concretes with Limestone Calcined Clay Cement (LC 3), 2018. (<https://doi.org/10.1016/j.cemconres.2018.02.005>). (<http://www.elsevier.com/locate/cemconres>).
- [7] A. Alujas Diaz, et al., Properties and occurrence of clay resources for use as supplementary cementitious materials: a paper of RILEM TC 282-CCL, Mater. Struct./Mater. et Constr. 55 (5) (2022), <https://doi.org/10.1617/s11527-022-01972-2>.
- [8] S. Bishnoi, et al., Pilot scale manufacture of limestone calcined clay cement: the Indian experience, Indian Concr. J. 88 (7) (2014) 22–28.
- [9] N. Beuntner, et al., Potential of calcined mixed-layer clays as pozzolans in concrete, ACI Mater. J. 116 (4) (2019) 19–29, <https://doi.org/10.14359/51716677>.
- [10] A. Ahlberg, et al., Triassic-Jurassic weathering and clay mineral dispersal in basement areas and sedimentary basins of southern Sweden, Sediment. Geol. 161 (1–2) (2003) 15–29, [https://doi.org/10.1016/S0037-0738\(02\)00381-0](https://doi.org/10.1016/S0037-0738(02)00381-0).
- [11] G. Plusquellec, et al., Activated clays as supplementary cementitious material, RISE report, 2020.
- [12] A. Hazarika, et al., Characterisation, activation, and reactivity of heterogeneous natural clays, Mater. Struct./Mat. et Constr., 2024. (<https://doi.org/10.1617/s11527-024-02335-9>).
- [13] M. Flegar, et al., Regional waste streams as potential raw materials for immediate implementation in cement production, Materials 13 (23) (2020) 1–15, <https://doi.org/10.3390/ma13235456>.
- [14] E.A. Costantini, D. Damiani, Clay minerals and the development of quaternary soils in central Italy, Rev. Mex. de Cienc. Geol. 21 (1) (2004) 144–159.
- [15] M. Setti, et al., Clay mineralogy in southern Africa river muds, Clay Miner. 49 (5) (2014) 717–733, <https://doi.org/10.1180/claymin.2014.049.5.08>.
- [16] I. Tole, Enhancing the pozzolanic activity of three natural clays from sweden by mechanochemical activation process, SSRN Electron. J. (2022) 0–2, <https://doi.org/10.2139/ssrn.4100172>.
- [17] V.A. Baki, et al., The impact of mechanochemical activation on the physicochemical properties and pozzolanic reactivity of kaolinite, muscovite and montmorillonite, Cem. Concr. Res. 162 (May) (2022) 106962, <https://doi.org/10.1016/j.cemconres.2022.106962>.
- [18] N. Beuntner, K. Thienel, Properties of Calcined Lias Delta Clay—Technological Effects, Physical Characteristics and Reactivity in Cement, RILEM Bookseries, 2015. (<https://doi.org/10.1007/978-94-017-9939-3>).
- [19] A. Játiva, et al., Volcanic ash as a sustainable binder material: an extensive review, Materials 14 (5) (2021) 1–32, <https://doi.org/10.3390/ma14051302>.
- [20] S.P. Jakobsson, M.T. Gudmundsson, Subglacial and intraglacial volcanic formations in Iceland, Jökull 58 (2008) 179–196.
- [21] K. Jónasson, Silicic volcanism in Iceland: composition and distribution within the active volcanic zones, J. Geodyn. 43 (1) (2007) 101–117, <https://doi.org/10.1016/j.jog.2006.09.004>.
- [22] S. Ekolu, et al., Proc. Int. Conf. Adv. Eng. Technol. (2006) 75–83, <https://doi.org/10.1016/b978-008045312-5/50009-1>.
- [23] S. Shoji, et al., Chapter 1 terminology, concepts and geographic distribution of volcanic ash soils, Dev. Soil Sci. 21 (C) (1993) 1–5, [https://doi.org/10.1016/S0166-2481\(08\)70262-9](https://doi.org/10.1016/S0166-2481(08)70262-9).
- [24] A. Wilson, et al., Volcanic and volcanoclastic rocks of the mesoarchaean pongola supergroup in South Africa and swaziland: distribution, physical characteristics, stratigraphy and correlations, South Afr. J. Geol. 116 (1) (2013) 119–168, <https://doi.org/10.2113/gssajg.116.1.119>.
- [25] G. Cai, Volcano-related materials in concretes: a comprehensive review, 2016, pp. 7220–43. (<https://doi.org/10.1007/s11356-016-6161-z>).
- [26] H.V. Cabadas-Báez, et al., Reworked volcanoclastic deposits from the Usumacinta river, Mexico: a serendipitous source of volcanic glass in Maya ceramics, Geoarchaeology 32 (3) (2017) 382–399, <https://doi.org/10.1002/zea.21610>.
- [27] Thomas Betong: First out in Sweden with the volcanic rock mixed in concrete. (<https://thomasconcretegroup.com/us/latest-news/first-out-in-sweden-with-the-volcanic-rock-mixed-in-concrete>).
- [28] Heidelberg Materials, Tuff processing in Thorlákshöfn. (<https://heidelberg.is/en/>).
- [29] G.M. Mortensen, et al., Alternativa bindemedel till betong, 2023. (<https://resource.sgu.se/dokument/publikation/rr/rr202302rapport/RR2302.pdf>).
- [30] B. Lothenbach, et al., Supplementary cementitious materials, Cem. Concr. Res. 41 (12) (2011) 1244–1256, <https://doi.org/10.1016/j.cemconres.2010.12.001>.
- [31] R. Siddique, Properties of concrete made with volcanic ash, Resour. Conserv. Recycl. 66 (2012) 40–44, <https://doi.org/10.1016/J.RESCONREC.2012.06.010>.
- [32] Svensk standard ss-en 197-1:2011, Tech. rep., Swedish Standards Institute, Stockholm, Sweden, 2011.
- [33] Svensk standard ss-en 197-5:2021, Tech. rep., Swedish Institute of Standards, Stockholm, Sweden, 2021.
- [34] A.S. Alqarni, A comprehensive review on properties of sustainable concrete using volcanic pumice powder ash as a supplementary cementitious material, Constr. Build. Mater. 323 (October 2021) (2022) 126533, <https://doi.org/10.1016/j.conbuildmat.2022.126533>.
- [35] K.M. Hossain, Blended cement using volcanic ash and pumice, Cem. Concr. Res. 33 (10) (2003) 1601–1605, [https://doi.org/10.1016/S0008-8846\(03\)00127-3](https://doi.org/10.1016/S0008-8846(03)00127-3).
- [36] K.M.A. Hossain, Blended cement and lightweight concrete using scoria: mix design, strength, durability and heat insulation characteristics, Int. J. Phys. Sci. 1 (1) (2006) 5–16.
- [37] K.M. Hossain, Performance of volcanic ash based precast and in situ blended cement concretes in marine environment, J. Mater. Civ. Eng. 17 (6) (2005) 694–702, [https://doi.org/10.1061/\(asce\)0899-1561\(2005\)17:6\(694\)](https://doi.org/10.1061/(asce)0899-1561(2005)17:6(694)).
- [38] K. Kupwade-Patil, et al., Microstructure of cement paste with natural pozzolanic volcanic ash and Portland cement at different stages of curing, Constr. Build. Mater. 113 (2016) 423–441, <https://doi.org/10.1016/j.conbuildmat.2016.03.084>.
- [39] K. Khan, et al., Effect of fineness and heat treatment on the pozzolanic activity of natural volcanic ash for its utilization as supplementary cementitious materials, Crystals 12 (2) (2022), <https://doi.org/10.3390/cryst12020302>.
- [40] P. Suraneni, et al., New insights from reactivity testing of supplementary cementitious materials, Cem. Concr. Compos. 103 (2019) 331–338, <https://doi.org/10.1016/j.cemconcomp.2019.05.017>.
- [41] L. Turanlı, B. Uzal, F. Bektas, Effect of material characteristics on the properties of blended cements containing high volumes of natural pozzolans, Cem. Concr. Res. 34 (12) (2004) 2277–2282, <https://doi.org/10.1016/j.cemconres.2004.04.011>.
- [42] J. Rosales, et al., Effect of processed volcanic ash as active mineral addition for cement manufacture, Materials 15 (18) (2022), <https://doi.org/10.3390/ma15186305>.
- [43] M.A. Sanjuán, et al., Volcanic ash from La Palma (Canary Islands, Spain) as Portland cement constituent, J. Build. Eng. 78 (July) (2023), <https://doi.org/10.1016/j.jobbe.2023.107641>.
- [44] S. Ahmad, et al., Influence of admixing natural pozzolan as partial replacement of cement and microsilica in UHPC mixtures, Constr. Build. Mater. 198 (2019) 437–444, <https://doi.org/10.1016/j.conbuildmat.2018.11.260>.
- [45] J.N. Yankwa Djobo, et al., Mechanical activation of volcanic ash for geopolymer synthesis: effect on reaction kinetics, gel characteristics, physical and mechanical properties, RSC Adv. 6 (45) (2016) 39106–39117, <https://doi.org/10.1039/c6ra03667h>.
- [46] H. Tang, et al., Effect of mechanical activation on hydration properties of natural volcanic rock towards partially replacing cement in composite cementitious materials, J. Build. Eng. 83 (2023) (2024) 108427, <https://doi.org/10.1016/j.jobbe.2023.108427>.
- [47] J.N.Y. Djobo, et al., Volcanic ash-based geopolymer cements/concretes: the current state of the art and perspectives, Environ. Sci. Pollut. Res. 24 (5) (2017) 4433–4446, <https://doi.org/10.1007/s11356-016-8230-8>.
- [48] P. Balaz, High-energy milling, in: Mechanochemistry in Nanoscience and Minerals Engineering, Springer-Verlag, Berlin Heidelberg, 2008, 2008.
- [49] P.J. Sanchez-Soto, et al., Effects of dry grinding on the structural changes of kaolinite powders, J. Am. Ceram. Soc. 57 (2000) 1649–1657.
- [50] T. Danner, et al., Reactivity of alternative SCMs from Nordic Countries – input for the R3 test, in: Proceedings of the 16th International Congress on the Chemistry of Cement, 2023, September.
- [51] R.T. Thorstensen, P. Fijdestøl, Inconsistencies in the pozzolanic strength activity index (SAI) for silica fume according to EN and ASTM, Mater. Struct./Mater. Constr. 48 (12) (2015) 3979–3990, <https://doi.org/10.1617/s11527-014-0457-6>.
- [52] M.C. Juenger, R. Siddique, Recent advances in understanding the role of supplementary cementitious materials in concrete, Cem. Concr. Res. 78 (2015) 71–80, <https://doi.org/10.1016/j.cemconres.2015.03.018>.
- [53] S. Donatello, et al., Comparison of test methods to assess pozzolanic activity, Cem. Concr. Compos. 32 (2) (2010) 121–127, <https://doi.org/10.1016/j.cemconcomp.2009.10.008>.



- [54] R. Pourkhorshidi, et al., A comparative study of the evaluation methods for pozzolans, *Adv. Cem. Res.* 22 (3) (2010) 157–164, <https://doi.org/10.1680/adcr.2010.22.3.157>.
- [55] X. Li, et al., Reactivity tests for supplementary cementitious materials: RILEM TC 267-TRM phase 1, *Mater. Struct./Mater. Constr.* 51 (6) (2018), <https://doi.org/10.1617/s11527-018-1269-x>.
- [56] D. Londono-Zuluaga, et al., Report of RILEM TC 267-TRM phase 3: validation of the R3 reactivity test across a wide range of materials, *Mater. Struct.* 55 (5) (2022), <https://doi.org/10.1617/s11527-022-01947-3>.
- [57] P. Suraneni, Recent developments in reactivity testing of supplementary cementitious materials, *RILEM Tech. Lett.* 6 (2021) 131–139, <https://doi.org/10.21809/rilemtechlett.2021.150>.
- [58] P. Pourghahramani, M.A. Azami, Mechanical activation of natural acidic igneous rocks for use in cement, *Int. J. Miner. Process.* 134 (2015) 82–88, <https://doi.org/10.1016/j.minpro.2014.12.001>.
- [59] A.T. Almalkawi, et al., One-part alkali activated cement based volcanic pumice, *Constr. Build. Mater.* 152 (2017) 367–374, <https://doi.org/10.1016/j.conbuildmat.2017.06.139>.
- [60] R. Szabó, et al., Reaction, structure and properties of eco-friendly geopolymer cement derived from mechanically activated pumice, *Ceram. Int.* 49 (4) (2023) 6756–6763, <https://doi.org/10.1016/j.ceramint.2022.10.204>.
- [61] T.J. Banik, et al., Magma-ice-sediment interactions and the origin of lava/hyaloclastite sequences in the Sía formation, South Iceland, *Bull. Volcanol.* 76 (1) (2014) 1–19, <https://doi.org/10.1007/s00445-013-0785-3>.
- [62] R. Dahlgren, et al., Chapter 5 mineralogical characteristics of volcanic ash soils, *Dev. Soil Sci.* 21 (C) (1993) 101–143, [https://doi.org/10.1016/S0166-2481\(08\)70266-6](https://doi.org/10.1016/S0166-2481(08)70266-6).
- [63] P. Hemstad, Cement Paste Chemistry and Its Relation to Concrete Durability (Doctoral thesis), Norwegian University of Science and Technology, Trondheim, 2023.
- [64] P. Hemstad, et al., The effect of varying cement replacement level on alkali metal distribution in cement pastes, *Cem. Concr. Compos.* 146 (October 2023) (2024) 105344, <https://doi.org/10.1016/j.cemconcomp.2023.105344>.
- [65] P. Zuschlag, The Impact of Curing Temperatures on Portland Composite Cements – Hydrate Assemblage, Porosity, and Compressive Strength (Doctoral thesis), Norwegian University of Science and Technology, Trondheim, 2022. (<https://ntnuopen.ntnu.no/ntnu-xmlui/handle/11250/3042301>).
- [66] P. Hemstad, et al., Alkali metal distribution in composite cement pastes and its relation to accelerated ASR tests, *Cem. Concr. Res.* 173 (May) (2023), <https://doi.org/10.1016/j.cemconres.2023.107283>.
- [67] A.G. Whitham, R.S. Sparks, Pumice, *Bull. Volcanol.* 48 (4) (1986) 209–223, <https://doi.org/10.1007/BF01087675>.
- [68] C. Frick, L.E. Kent, Drift pumice in the Indian and South Atlantic Oceans, *South Afr. J. Geol.* 87 (1984) 19–33, <https://doi.org/10.10520/EJC-1158c3dad3>.
- [69] M. Piochi, et al., Texture and composition of pumices and scoriae from the Campi Flegrei caldera (Italy): implications on the dynamics of explosive eruptions, *Geochim. Geophys. Geosyst.* 9 (3) (2008), <https://doi.org/10.1029/2007GC001746>.
- [70] P.N. Lemougna, et al., Review on the use of volcanic ashes for engineering applications, *Resour. Conserv. Recycl.* 137 (2018) 177–190, <https://doi.org/10.1016/J.RESCONREC.2018.05.031>.
- [71] K.M. Hossain, M. Lachemi, Performance of volcanic ash and pumice based blended cement concrete in mixed sulfate environment, *Cem. Concr. Res.* 36 (6) (2006) 1123–1133, <https://doi.org/10.1016/j.cemconres.2006.03.010>.
- [72] R. Snellings, et al., Future and emerging supplementary cementitious materials, *Cem. Concr. Res.* 171 (2023), <https://doi.org/10.1016/j.cemconres.2023.107199>.
- [73] S. Venkatram, et al., A close look at polymer degree of crystallinity versus polymer crystalline quality, *Polym. Int.* 72 (10) (2023) 855–860, <https://doi.org/10.1002/pi.6508>.
- [74] İ. Uzun, Methods of determining the degree of crystallinity of polymers with X-ray diffraction: a review, vol. 30, 2023. (<https://doi.org/10.1007/s10965-023-03744-0>).
- [75] T. Serbouce, et al., The glassy structure of reactive supplementary cementitious materials (SCMs) and recycled glass: contribution of XRD and Raman spectroscopy to their characterization, *Cem. Concr. Res.* 179 (February) (2024), <https://doi.org/10.1016/j.cemconres.2024.107468>.
- [76] T. Monecke, et al., Quantitative phase-analysis by the Rietveld method using X-ray powder-diffraction data: application to the study of alteration halos associated with volcanic-rock-hosted massive sulfide deposits, *Can. Mineral.* 39 (6) (2001) 1617–1633, <https://doi.org/10.2113/gscammin.39.6.1617>.
- [77] X. Zhou, et al., XRD-based quantitative analysis of clay minerals using reference intensity ratios, mineral intensity factors, Rietveld, and full pattern summation methods: a critical review, *Solid Earth Sci.* 3 (1) (2018) 16–29, <https://doi.org/10.1016/j.sesci.2017.12.002>.
- [78] R. Snellings, et al., Paper of RILEM TC 282-CCL: Mineralogical Characterization Methods for Clay Resources Intended for Use as Supplementary Cementitious Material, Springer Netherlands, 2022 (Vol. 1, (<https://doi.org/10.1617/s11527-022-01973-1>)).
- [79] R. Snellings, et al., Report of TC 238-SCM: hydration stoppage methods for phase assemblage studies of blended cements—results of a round robin test, *Mater. Struct./Mater. Constr.* 51 (4) (2018), <https://doi.org/10.1617/s11527-018-1237-5>.
- [80] M.A. Bérubé, et al., Effects of lime on common soil and rock forming minerals, *Appl. Clay Sci.* 5 (2) (1990) 145–163, [https://doi.org/10.1016/0169-1317\(90\)90020-P](https://doi.org/10.1016/0169-1317(90)90020-P).
- [81] C. Svanholm, Origin of silicic magmatism at the Katla volcano, South Icel. (2021).
- [82] M.A. Mast, J.I. Drever, The effect of oxalate on the dissolution rates of oligoclase and tremolite, *Geochim. Cosmochim. Acta* 51 (9) (1987) 2559–2568, [https://doi.org/10.1016/0016-7037\(87\)90306-1](https://doi.org/10.1016/0016-7037(87)90306-1).
- [83] E.H. Oelkers, et al., Olivine dissolution rates: a critical review, *Chem. Geol.* 500 (October) (2018) 1–19, <https://doi.org/10.1016/j.chemgeo.2018.10.008>.
- [84] P. Westgate, et al., Olivine as a reactive aggregate in lime mortars, *Constr. Build. Mater.* 195 (2019) 115–126, <https://doi.org/10.1016/j.conbuildmat.2018.11.062>.
- [85] C.H. Lee, Solid state reduction and magnetic properties of iron oxide-iron system induced by ball milling process, *Korean J. Mater. Res.* 34 (6) (2024) 309–314, <https://doi.org/10.3740/MRSK.2024.34.6.309>.
- [86] K. Tokumitsu, et al., Deoxidation of iron oxide by ball-milling, *Mater. Sci. Forum* 269–272 (PART 1) (1998) 181–186, <https://doi.org/10.4028/www.scientific.net/msf.269-272.181>.
- [87] T. Nasu, et al., Reduction of iron-oxide by ball-milling with hydrogen gas flow, *Mater. Sci. Forum* 343 (2000) 435–440, <https://doi.org/10.4028/www.scientific.net/msf.343-346.435>.
- [88] S.J. Blott, et al., Particle size analysis by laser diffraction, *Geol. Soc. Spec. Publ.* 232 (2004) 63–73, <https://doi.org/10.1144/GSL.SP.2004.232.01.08>.
- [89] H. He, K. Senetakis, An experimental study on the micromechanical behavior of pumice, *Acta Geotech.* 14 (6) (2019) 1883–1904, <https://doi.org/10.1007/s11440-019-00867-x>.
- [90] C. Zanelli, et al., Mineralogical composition and particle size distribution as a key to understand the technological properties of Ukrainian ball clays, *Appl. Clay Sci.* 108 (2015) 102–110, <https://doi.org/10.1016/j.clay.2015.02.005>.
- [91] S. Al-Shmaisani, et al., Critical assessment of rapid methods to qualify supplementary cementitious materials for use in concrete, *Cem. Concr. Res.* 153 (October 2021) (2022) 106709, <https://doi.org/10.1016/j.cemconres.2021.106709>.
- [92] Y. Wang, et al., Reactivity of unconventional fly ashes, SCMs, and fillers: effects of sulfates, carbonates, and temperature, in: *Advances in Civil Engineering Materials under rev.*, no. August, 2022. (<https://doi.org/10.1520/ACEM20220003>).
- [93] J. Skibsted, R. Snellings, Reactivity of supplementary cementitious materials (SCMs) in cement blends, *Cem. Concr. Res.* 124 (June) (2019) 105799, <https://doi.org/10.1016/j.cemconres.2019.105799>.
- [94] C. Hu, Z. Li, A review on the mechanical properties of cement-based materials measured by nanoindentation, *Constr. Build. Mater.* 90 (2015) 80–90, <https://doi.org/10.1016/j.conbuildmat.2015.05.008>.
- [95] F. Song, et al., The effects of crystallinity on the mechanical properties and the limiting PV (pressure × velocity) value of PTFE, *Tribol. Int.* 93 (2016) 1–10, <https://doi.org/10.1016/j.triboint.2015.09.017>.

- [96] G. Yao, et al., Pozzolanic activity and hydration properties of feldspar after mechanical activation, *Powder Technol.* 383 (2021) 167–174, <https://doi.org/10.1016/j.powtec.2021.01.042>.
- [97] E.C. Sánchez, et al., Effects of grinding of the feldspar in the sintering using a planetary ball mill, *J. Mater. Process. Technol.* 152 (3) (2004) 284–290, <https://doi.org/10.1016/j.jmatprotec.2004.04.367>.
- [98] K. Sæmundsson, M.Á. Sigurgeirsson, G.Ó. Fridleifsson, Geology and structure of the Reykjanes volcanic system, Iceland, *J. Volcanol. Geotherm. Res.* (2018), <https://doi.org/10.1016/j.jvolgeores.2018.11.022>.
- [99] H. Tómasson, Jökulhlaup from Katla in 1918, *Ann. Glaciol.* 22 (1996) 249–254.
- [100] G. Larsen, Katla: tephrochronology and eruption history, *Dev. Quat. Sci.* 13 (2010) 23–49.
- [101] G. Larsen, S. Thorarinsson, H-4 and other acid Hekla tephra layers, *Jökull* 27 (1977) 28–46.
- [102] S.O.B.A. Óladóttir, G. Larsen, T. Thordarson, The Katla volcano S-Iceland: Holocene tephra stratigraphy and eruption frequency, *Jökull* 55 (2005) 53–74.
- [103] G.B.M. Pedersen, P. Grosse, Morphometry of subaerial shield volcanoes and glaciovolcanoes from Reykjanes Peninsula, Iceland: effects of eruption environment, *J. Volcanol. Geotherm. Res.* 282 (2014) 115–133, <https://doi.org/10.1016/j.jvolgeores.2014.06.008>.